RSC Advances

REVIEW

View Article Online
View Journal | View Issue

Cite this: *RSC Adv.*, 2022, **12**, 28227

Recent development and challenges in fuel cells and water electrolyzer reactions: an overview

Rasu Ramachandran,[a] Tse-Wei Chen,[b] Pitchaimani Veerakumar,[c] Ganesan Anushya,[d] Shen-Ming Chen,[e] Ramanjam Kannan,[f] Vinitha Mariyappan,[e] Selvam Chitra,[g] Nagappan Ponmurugaraj[h] and Muthusamy Boominathan[a]

Water electrolysis is the most promising method for the production of large scalable hydrogen (H_2), which can fulfill the global energy demand of modern society. H_2-based fuel cell transportation has been operating with zero greenhouse emission to improve both indoor and outdoor air quality, in addition to the development of economically viable sustainable green energy for widespread electrochemical applications. Many countries have been eagerly focusing on the development of renewable as well as H_2-based energy storage infrastructure to fulfill their growing energy demands and sustainable goals. This review article mainly discusses the development of different kinds of fuel cell electrocatalysts, and their application in H_2 production through various processes (chemical, refining, and electrochemical). The fuel cell parameters such as redox properties, cost-effectiveness, ecofriendlyness, conductivity, and better electrode stability have also been highlighted. In particular, a detailed discussion has been carried out with sufficient insights into the sustainable development of future green energy economy.

Received 4th August 2022
Accepted 1st September 2022

DOI: 10.1039/d2ra04853a

rsc.li/rsc-advances

[a]*Department of Chemistry, The Madura College, (Madurai Kamaraj University) Vidhya Nagar, T.P.K. Road, Madurai 625011, India. E-mail: ramachandran@maduracollege.edu.in*

[b]*Department of Materials, Imperial College London, London SW7 2AZ, UK*

[c]*Department of Chemistry, National Taiwan University, Taipei 10617, Taiwan. E-mail: spveerakumar@gmail.com*

[d]*Department of Physics, St. Joseph College of Engineering, Sriperumbudur, Chennai 602117, India*

[e]*Electroanalysis and Bio-electrochemistry Laboratory, Department of Chemical Engineering and Biotechnology, National Taipei University of Technology, Taipei 106, Taiwan. E-mail: smchen78@ms15.hinet.net*

[f]*Department of Chemistry, Sri KumaraguruparaSwamigal Arts College, Srivaikuntam, Thoothukudi-628619, India*

[g]*Department of Chemistry, Alagappa Government Arts College, Karaikudi 630003, India*

[h]*Department of Chemistry, S.T.Hindu College, Nagercoil 629002, India*

Dr Rasu Ramachandran is Assistant Professor of Chemistry, Madura College, Madurai, Tamil Nadu, India. He obtained his doctoral degree from Madurai Kamaraj University, Madurai, India. He visited Prof. Shen-Ming Chen Laboratory, Department of Chemical Engineering and Biotechnology, National Taipei University of Technology, Taipei, Taiwan. He has published more than 40 articles in reputed scientific journals and contributed few chapters in books. His main research areas include the design and development of novel electrodes and polymer nanocomposites applicable for a number of electrochemical applications including fuel cells, sensors, and energy storage applications.

Mr Tse-Wei Chen is currently a PhD student in Department of Material Science at Imperial College London. He received M.Sc. (2018) degree in Chemical Engineering from National Taipei University of Technology, Taiwan. His research interest includes nano-based catalyst synthesis and application for renewable energy device, electrochemical sensors, and biosensors.

1. Introduction

In a modern society, green and clean energy storage and conversion technologies are promising for devices as they can operate with high efficiency. In this type of device, chemical energies are directly converted into fuels (electrical energy) with zero emission and high efficiencies compared to combustion engines. Fuel cells are a major hopeful storage device technology, which fulfill the global energy demand and reduce environmental pollution.[1,2] In general, the use of fossil fuels is polluting the environment. For this reason, many countries are gradually replacing fossil fuels; consequently, researchers are mainly focused on the development of green energy storage devices, which fulfill the energy requirements.[3] They are attractive clean energy resources with wider range of electrical applications. Also, they exhibit good thermal, electrical, mechanical stability, easy transport, high energy density as well as greater efficiency with excellent electrical conductivity during operation.[4] However, the overall fuel cell efficiencies are mainly dependent on the nature of electrocatalysts and could be favorable due to a larger electrode surface area, high electron affinity, and less cost with beneficial mechanical stability.[5] Different kinds of energy storage devices are commonly developed, which can be used as potential candidates in automobile applications, such as batteries, solar cells, fuel cells, water electrolyzers, and supercapacitors.[6–10] Typically, energy storage devices have higher energy density than others and usually have

Dr Pitchaimani Veerakumar obtained his M.Sc. (2004), M.Phil., (2007), and PhD (2012) under the supervision of Prof. S. Rajagopal, School of Chemistry, Madurai Kamaraj University, Madurai, India. In 2012–2016, he worked as a postdoctoral research researcher at Institute of Atomic and Molecular Sciences, Academia Sinica (Prof. Shang-Bin Liu), Taiwan. He worked as a Senior Postdoctoral Fellow (2016–2022) from the Department of Chemistry, National Taiwan University (Prof. King-Chuen Lin), Taiwan. His research interests include the preparation of highly porous carbons derived from biomass, metal-free catalysts, sustainable organic transformations, electrochemical sensors, adsorption of toxic materials, supercapacitors, and photodegradation of pesticides.

Dr Ganesan Anushya is currently working as Assistant Professor in the Department of Physics at St. Joseph College of Engineering, Chennai, India. She obtained her PhD in Physics from M.S. University, Tirunelveli, in 2020. She has published more than 15 papers in refereed international Journals and presented more than 10 papers at various international/national conferences. Her research interests include nanomaterials, biomaterials science, crystal growth, and sensors.

Prof. Shen-Ming Chen received his B.S. Degree in Chemistry in 1980 from National Kaohsiung Normal University, Taiwan. He received his M.S. Degree (1983) and PhD degree (1991) in Chemistry from National Taiwan University, Taiwan. He is currently a professor at the Department of Chemical Engineering and Biotechnology, National Taipei University of Technology, Taiwan. His current research interests include electroanalytical chemistry, bioelectrochemistry, fabrication of energy conservation and storage devices, and nanomaterial synthesis for electrochemical applications. He has published above 1200 papers in SCI journals.

Dr Ramanjam Kannan obtained his undergraduate degree in chemical science from Madurai Kamaraj University (India), postgraduate degree in chemical science from Gandhigram University (India), and received his doctoral degree from Anna University (India) in 2013. Then, he continued his postdoctoral research with the Prof. Dong Jin Yoo's group in Chonbuk National University, RoK. In 2015, he was selected for the Korean Research Fellow programme and worked as Assistant Professor at the Department of Energy Storage and Conversion, Chonbuk National University, RoK. He is presently working as Assistant Professor at Sri Kumaragurupara Swamigal Arts College, Srivaikuntam, Thoothukudi Dist, India. His research interests include fuel cells, catalysis, biosensors, and photochemical reactions.

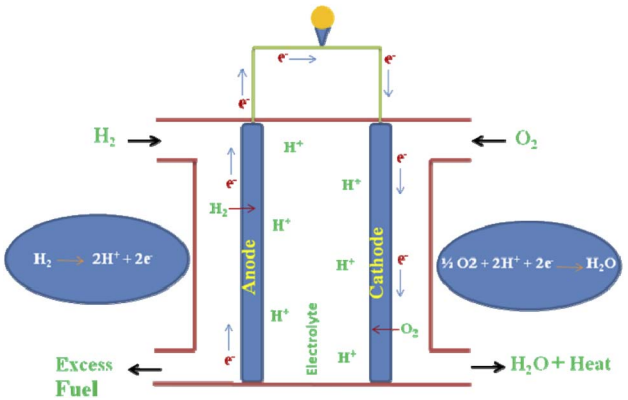

Fig. 1 Schematic representation of the reaction mechanism of a fuel cell.

operating ranges from more than 300 km per charge, while their recharging time is ~2 h or more.[11] H_2 fuel cells have been considered as potential energy storage devices and can be used as an alternative of fossil fuels. There will be huge challenges in various aspects such as difficulties in the transport and storage process.[24] Similarly, the low-density nature of H_2 fuel cells is a great challenge in its distribution, bulk storage, and on-board vehicle storage process,[25] despite the impressive progress that has been made for the sustainable development of clean H_2 production through electrochemical WS under alkaline conditions with constructed novel active surface-based nanocomposite materials. The principle of the fuel cell reaction and the process have been highlighted in Fig. 1.

Many countries have promoted both H_2 and fuel cell technologies to meet the global energy demands and develop technological strategies. H_2 can play an important role in energy storage strategies and can act as a potential candidate, which can be widely applied in virtually all sectors such as commercial, residential, transportation, industrial, and portable electronics.[18] However, much emphasis has been put on the production of zero carbon emission sustainable H_2 using through wind, solar cell, and hydrothermal (HT) energy as the power sources. Water electrolysis is the key process, in which water (H_2O) is split into H_2 and oxygen (O_2) through efficient strategies. H_2 energy has high purity, stable output, high mass density, and feasible for large scale production due to the renewable energy sources used.[12–14] Hence, extensive effort has been made for the development of water splitting (WS) reactions to generate efficient H_2 energy.[15–18] Most importantly, water electrolysis is an interesting and innovative H_2 generation technique due to the purity of the product and its simplicity. In

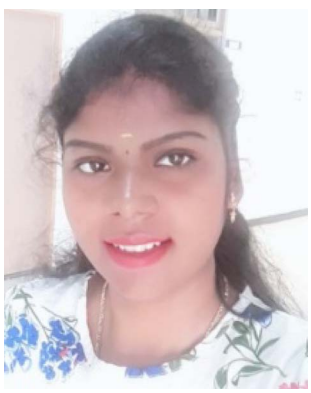

Dr Vinitha Mariyappan received her B.Sc. (2015) and M.Sc. (2017) degrees in chemistry from The Madura College, Madurai, Tamil Nadu, India. Her doctoral degree was awarded in the year 2022 by the Department of Chemical Engineering and Biotechnology, National Taipei University of Technology, Taiwan. She has published more than 25 research articles in SCI journals. Her research interest is mainly focused on electrochemical sensors, biosensors, fuel cells, and energy applications.

Dr Selvam Chitra is Assistant Professor of Chemistry, Alagappa Government Arts and Science College, Karaikudi, Tamil Nadu, India. She obtained her doctoral degree from Alagappa University, Karaikudi. Her research interest includes the design and development of carbon-based nanocomposite electrode materials for electrochemical applications and green synthesis of heterocyclic compounds.

Dr. Nagappan Ponmurugaraj is Assistant Professor, Department of Chemistry, S. T. Hindu College, Nagercoil, Tamil Nadu, India. He obtained his doctoral degree from Manonmaniam Sundaranar University, Tirunelveli. His research interest includes the design and development of physical chemistry-based heavy metal analysis for physical applications.

Dr. Muthusamy Boominathan is Assistant Professor, Department of Chemistry, Madura College, Madurai, Tamil Nadu, India. He obtained his doctoral degree from Madurai Kamaraj University. His research interests include organic synthesis and the design and development of nanomaterials for catalytic applications.

general, the overall WS reactions performances are mainly dependent on the nature of the half-cell reactions of both the hydrogen evolution reaction (HER) and oxygen evolution reaction (OER) at the cathode and anode, respectively.[19] Traditionally, metal-based electrocatalysts have been used as an important state-of-the art to improve the WS efficiency for both OER and HER.[20] Most prominently, cost-effective electrocatalysts have been widely used to boost catalysis and have been largely investigated as potential bifunctional catalysts for alkaline WS reactions.[21] More recently, extensive effort has been made for the development of environment-friendly, low-cost, and open-structure FeOOH-based electrocatalysts for the water oxidation process.[22] Significant progress has been made in the development of H_2 and solid oxide fuel cells, which exhibit a slow start-up process, are operated at both low and high temperature conditions, and are an efficient energy storage device.[23]

Most importantly, H_2 fuel cells have high operation temperature, high cost, and slow start-up process. They have huge challenges in various aspects such transport as well as storage.[24] Furthermore, due to the low density of the fuel cell, there can be a huge challenge in its bulk storage, distribution, and vehicle storage.[25] In particular, several researchers are paying considerable interest to fabricate an alternative high performance-based electrode material for the production of renewable energy resources. Furthermore, the fundamentals of fuel cells and their operation mechanism are also discussed in detail (Fig. 1).

In this review article, we have mainly focused on the key components of principles of fuel cells, WS mechanism, electrode fabrication processes, and tests for their electrocatalytic properties through advanced electrochemical techniques. Subsequently, the electrocatalytic behavior of nanocomposite materials, which generally depends on the nature of the exposed active sites, and their prospects and challenges of outstanding energy storage, and H_2 and O_2 generation through WS process, have also been discussed.

2. Nanostructured electrocatalysts

The principles and design techniques for the preparation of nanostructured materials for electrocatalysts are discussed here, including the simple and novel chemistry-based preparation approaches for nanostructured electrocatalysts. The different types of electrode materials have been demonstrated to promote their electrochemical activity owing to their unique size, diverse morphologies and the excellent electrochemical properties of the molecules.[26] In specific, nanosized catalysts are of prime importance as they are cost-effective, have a larger electrode surface area, and the long durability of catalytic materials help to speed up the electrochemical redox reactions.[27] On the other hand, recently, nanocomposite materials have received great attention in energy conversion and energy storage technologies (fuel cells and WS process).[28] Among them, WS electrochemical technologies dominate, which facilitates the three important electrochemical processes including OER,[29] HER,[30] and oxygen reduction reaction (ORR).[31] Due to the high cost and non-availability of noble metal catalysts, great efforts have been made to develop non-precious metal-based (NPM) electrocatalysts. Also, these catalysts exhibit high performance in fuel cell electrocatalysis and the WS process.[32] Recent studies have shown that heteroatom-doped carbon-based electrocatalysts have received much attention because of their high electrical conductivity, intrinsic electronic structure, and excellent chemical stability.[33] Herein, the high performance-based Co_3FeP_x@NF bifunctional electrocatalysts have gained a significant WS system, with an applied cell voltage value of 1.35 V and the achieved current density of 10 mA cm^{-2}.[34] There is a growing interest in the fabrication of iridium nanoparticle-supported N-doped graphene (Ir@N-G-600) composite that has demonstrated an impressive electrocatalytic activity for OER, HER, and WS reaction in both alkaline and acidic conditions. The as-fabricated Ir@N-G-600 bi-functional catalyst, which exhibits a strong interaction between Ir- and N-doped graphene, could enhance the overall WS process.[35] An efficient, inexpensive, and heterojunction-based bifunctional CoP/$CoCr_2O_4$ electrocatalyst was developed through a nanoscating-phosphorization route. Moreover, the heterojunctioned CoP/$CoCr_2O_4$ catalyst leads to phase separation and transformation with attractive structural properties. The CoP/$CoCr_2O_4$ catalyst also exhibited excellent electrocatalytic activities for both HER and OER reactions with their respective overpotential values of 290 and 212 mV, respectively, to achieve their current density value of 10 mA cm^{-2} under alkaline (1.0 M KOH) conditions (Fig. 2).[36]

Ji *et al.*[37] prepared a bifunctional carbonaceous material of graphitic carbon nitrite-based carbon nanofiber (g-CN-CNF) catalyst by the HT method. The resulting g-CN-CNF catalyst was studied for both ORR and OER activities in alkaline conditions. Much effort has been made in the development of three-dimensional macroporous-based multifunctional boron-doped nickel (B-Ni) catalyst, which was prepared by a facile

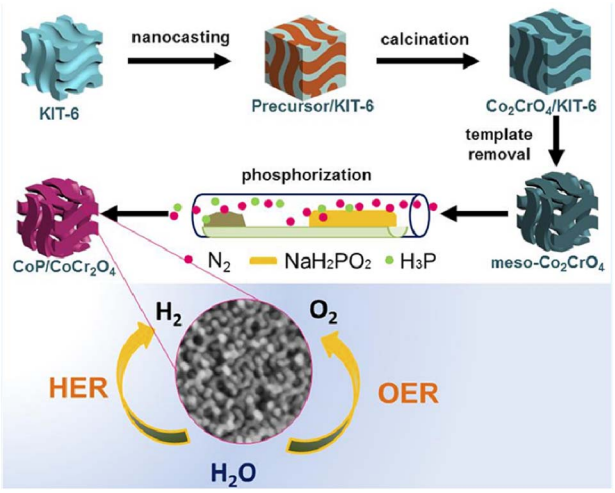

Fig. 2 Schematic illustration of the synthetic strategy of the mesoporous CoP/$CoCr_2O_4$ heterojunction for the HER measured in 1.0 M KOH solution. Reproduced with permission from ref. 36. Copyright 2020 American Chemical Society.

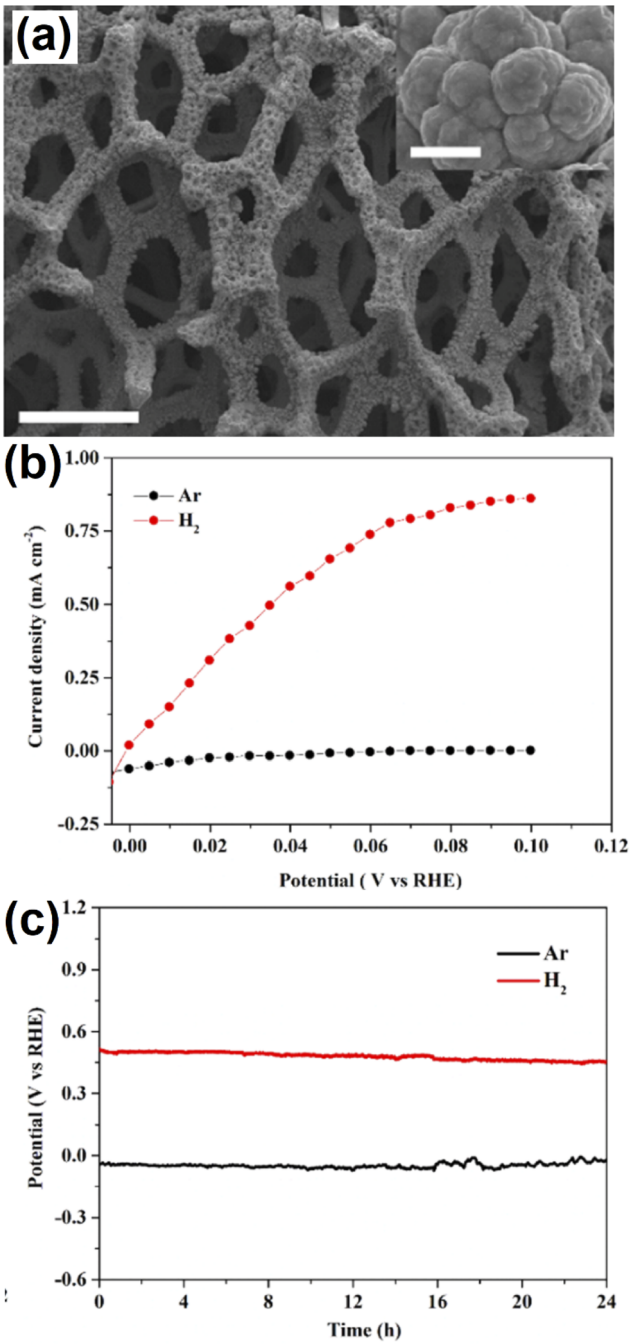

Fig. 3 (a) SEM image of B-Ni, (b) Steady-state polarization curves of B-Ni for the HOR in Ar- and H_2-saturated 0.1 M KOH, and (c) Chronoamperometry curves of B-Ni in Ar- and H_2-saturated 0.1 M KOH measured at 0.10 V *versus* RHE. Reproduced with permission from ref. 38. Copyright 2021 American Chemical Society.

route (Fig. 3a). However, the designed B-Ni catalyst showed outstanding H_2 oxidation reaction (HOR) activities through polarization curve studies and their long-term stability for B-Ni under alkaline conditions (Fig. 3b and c).[38]

Fan and co-workers[39] designed a nickel-based electrocatalyst through the carbonization process. Herein, the electrocatalysts displayed excellent electrocatalytic activity with impressive durability for H_2 evolution reaction, and exhibited a current density value of 1.2 mA cm^{-2}. The interesting Fe-doped Ni_2P nanosheets were prepared *via* the HT method, followed by the phosphorization process. The as-prepared structural engineered Fe-Ni_2P nanosheet could achieve the OER activity with a favorable potential value of 213 mV@100 mA cm^{-2}. Similarly, the HER performances also achieved their low cell voltage of 1.5 V@10 mA cm^{-2} with their remarkable stability.[40]

3. Metal-free electrocatalysts

In general, metal-based electrodes have been widely used in various electrochemical applications, such as electrochemical sensors,[41] biosensors,[42] batteries,[43] and fuel cells.[44] But these types of electrocatalysts suffer from various electrochemical parameters such as poor stability, low selectivity, and high adsorption of poisonous intermediates over the alternative electrocatalysts.[45] Therefore, researchers interested in developing either replace the metal catalyst or reduce the percentage of the metal in the catalyst; the above processes provide promising results in various electrochemical applications.[46,47] Cost-efficient and smooth surfaced iron-supported graphitic carbon nitride ($Fe_xCo_{1-x}Se_2$/g-C_3N_4) composite was prepared by a simple HT technique. The porous smooth nodular morphology of the $Fe_{0.2}Co_{0.8}Se_2$/g-C_3N_4 electrocatalysts exhibited uniform sphere-like structures and also showed excellent electrocatalytic activities toward robust HER and OER with good performance overpotentials of 193 and 450 mV s^{-1}, respectively.[48] The most versatile iron-based sulfide $(Fe_{0.2}Ni_{0.8})_{0.96}S$ bifunctional electrocatalyst was prepared *via* vulcanizing FeNi-

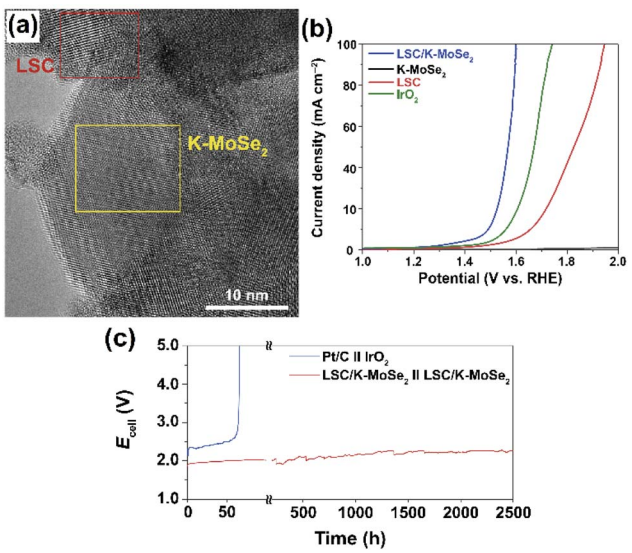

Fig. 4 (a) The HR-TEM image of LSC/K–$MoSe_2$, showing typical morphological characteristics of the heterostructure comprising the LSC (red square) and K–$MoSe_2$ (yellow square) regions, (b) Electrocatalytic HER and OER performances of LSC/K–$MoSe_2$, K–$MoSe_2$, and LSC; and (c) LSV and chronopotentiometric durability curves of Pt/C||IrO_2 and LSC/K–$MoSe_2$||LSC/K–$MoSe_2$ measured in 1 M KOH. All experiments recorded in N_2-saturated 1 M KOH at a scan rate of 5 mV s^{-1}. Reproduced with permission from ref. 50. Copyright 2021 Springer Nature.

LDH electrode grown on Ni foam. Finally, the assembled iron-based tubular sphere ($(Fe_{0.2}Ni_{0.8})_{0.96}S$ TSs/Ni) composite owing to its rich inner defects reflects more active sites and also displays the strong electron interaction between Fe, S, and Ni to improve the electrocatalytic properties for both OER and HER reactions. Furthermore, the self-assembled $(Fe_{0.2}Ni_{0.8})_{0.96}S$ which can be applied in alkaline electrolytes for WS reactions, gave a current density of 10 mA cm^{-2} with the achieved cell voltage of 1.56 V.[49] A robust bifunctional perovskite-supported potassium iron-bond molybdenum selenide ($La_{0.5}Sr_{0.5}CoO_{3-\delta}$, LSC/K–$MoSe_2$) composite was prepared by the ball-milling process. The HR-TEM micrographs confirm that all the components are uniformly distributed on the heterostructured electrocatalyst (Fig. 4a). For the heterostructured LSC/K–$MoSe_2$ electrocatalyst, the reaction kinetics and the WS process efficiency of the OER reaction displayed a remarkable electrode stability over 2500 h, with an applied current density of 100 mA cm^{-2} (Fig. 4b and c).[50]

Recently, non-precious bifunctional electrode materials were developed through a facile HT technique. Further, the photoanode of molybdenum-doped bismuth vanadate (MXene@C/BVO) was prepared through the sol-gel method, followed by the spin-coating method (Fig. 5a). The core–shell structure of MXene@C/BVO nanodots was analyzed by HR-TEM; the estimated core–shell had an average thickness of 1.6 nm (Fig. 5b). However, the electrochemical properties of the MXene@C/BVO electrocatalyst exhibited outstanding HER activities under different pH conditions (Fig. 5c). At pH 14, MX@C achieves a low onset potential of 134 mV at 10 mA cm^{-2} and reduced Tafel slope of 32 mV dec^{-1} due to facilitated charge transfer in the recombination reaction. However, the constructed MX@C/Mo : $BiVO_4$ photoanode showed an enhanced current density from 0.78 to 1.23 mA cm^{-2} with long-term durability over 8 h. These results were attributed to the facile surface catalytic kinetics of the chemically- and electronically-coupled MX@C hybrid at the heterointerface for both OER and HER.[51] Swesi *et al.*[52] grew a bifunctional NiSe electrocatalyst by a two-step process such as HT followed by electrodeposition. The efficient nanostructured $NiSe_2$ film acts as a superior electrocatalyst toward WS reactions and exhibits an energy efficiency of 83% at 100 mA cm^{-2}. This is due to the scaling of the Ni lattice plane as well as the increased covalency of the selenide lattice.

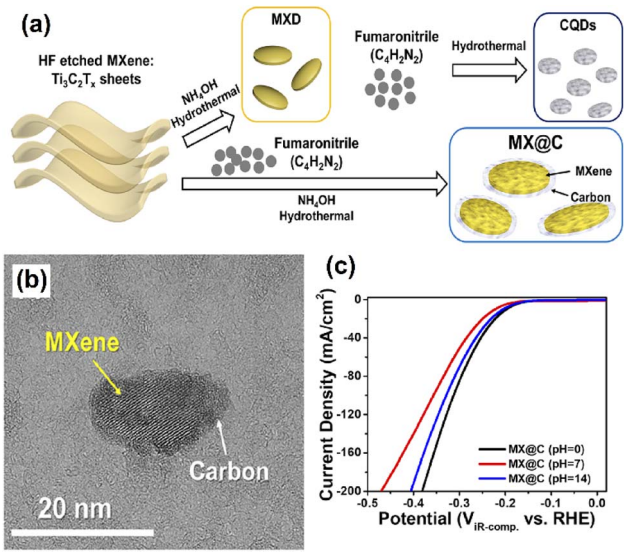

Fig. 5 (a) Schematic illustration of the synthesis of MXDs, CQDs, MX@C, and CQD-MXD, (b) HR-TEM images of MX@C and (c) polarization curves of MX@C at pH 0, 7, and 14. Reproduced with permission from ref. 51. Copyright 2020 American Chemical Society.

4. Metal sulfide-based electrocatalysts

In general, metal oxides play vital role in the development of energy storage and conversion technologies.[53] However, heterogenous electrocatalysts based on transition metal sulfides (TMS) are being actively explored in renewable energy research because nanostructured forms support high intrinsic activities for both HER and OER.[54] However, these types of noble metal oxides such as RuO_2 and IrO_2 are high in cost and have scarce natural resources. Recently, TMS-based electrocatalysts have emerged as the potential candidate for electrochemical HER/OER studies because of their unique physical and chemical properties and also because the electrodes depassivate their electrode surface to enhance their energy storage properties.[55] Nanostructured metal sulfide electrocatalysts hold great promise, offering larger surface-to-volume ratio, high specific capacitance/capacitivity, and multiple times greater energy efficiency than that of carbon-based electrocatalysts.[56] The monophase of cobalt sulfide (CoS_2)-based MOF was synthesized by the hydrothermal method, and a cobalt Prussian blue analogue (Co-PBAs, $Co_3[Co(CN)_6]_2$) was used as the starting material, after the process was over. The Co-PBAs were sulfurized under thermal conditions for the removal of some organic linkers from the MOFs. Finally, a bifunctional highly active catalyst was used for the mass production of mono-phase Co-PBAs. The uniformly porous MOF-derived CoS_2 exhibited

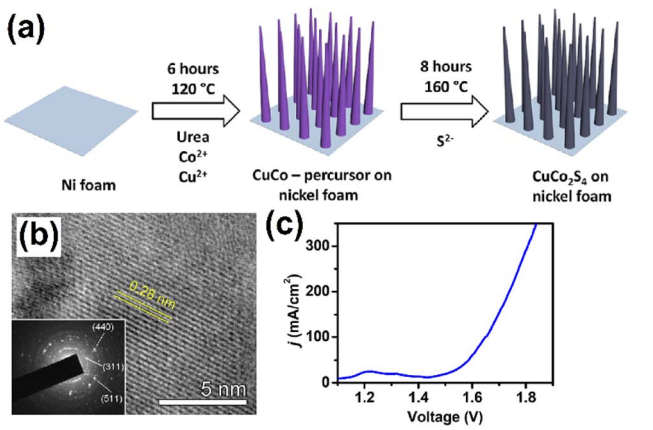

Fig. 6 (a) Schematic illustration of the formation of $CuCo_2S_4$ nanowire arrays on nickel foam, (b) HR-TEM image of $CuCo_2S_4$ with the SAED image in the inset, (c) the overall WS of $CuCo_2S_4$/NF: polarization curve (without *iR* compensation) of $CuCo_2S_4$/NF//$CuCo_2S_4$/NF at a scan rate of 5 mV s^{-1}. Reproduced with permission from ref. 59. Copyright 2018 American Chemical Society.

better electrochemical performance in the WS reaction, with the applied operating OER reaction potential of 298 mV @ 10 mA cm^{-2}.[57] On the other hand, the sulfide-supported metallic monoclinic 1T phase MoS_2 electrocatalyst was designed through an accessible two-step solvothermal method, followed by hydrolysis. The suggested that the 1T-MoS_2 electrocatalyst holds promising catalytically active sites, fast mass transport properties, and fascinating energy efficiency for the energy storage system.[58] The hierarchical $CuCo_2S_4$ electrocatalyst was synthesized by Steffen Czioska by a two-step hydrothermal method (Fig. 6a). The HR-TEM image of the $CuCo_2S_4$ nanowire morphology shows a lattice diameter of 0.28 nm, attributed to the diffraction plane of [311], which is highlighted through the selected area electron diffraction (SAED) patterns (Fig. 6b). The resultant $CuCo_2S_4$ bifunctional electrocatalyst was a high performance-based catalyst for OER under alkaline conditions at an applied electrode potential of 310 mV and an achieved current density of 100 mA cm^{-2} (Fig. 6c).[59]

Similarly, copper iron sulfide ($CuFeS_2$) bifunctional electrocatalyst was developed through a one-pot hydrothermal route, with $CuCl_2 \cdot 2H_2O$, $FeCl_2 \cdot 4H_2O$, and thiourea used as precursors. The microflower-like morphological structure of $CuFeS_2$ was observed by the FE-SEM technique (Fig. 7a). The demonstrated flower-like sulfide catalyst could drive the WS reaction for the production of clean H_2 fuel energy. A linear sweep voltammetric analysis of the $CuFeS_2$ electrocatalyst demonstrated its superior electrocatalytic activities for effectively driving HER and OER with lower overpotentials (η_{10}) of 136 and 320 mV in 1.0 M KOH electrolyte, respectively (Fig. 7b).[60]

The one-pot HT strategy has been used for the synthesis of the Ni/NiS heteronanoparticle morphology-based

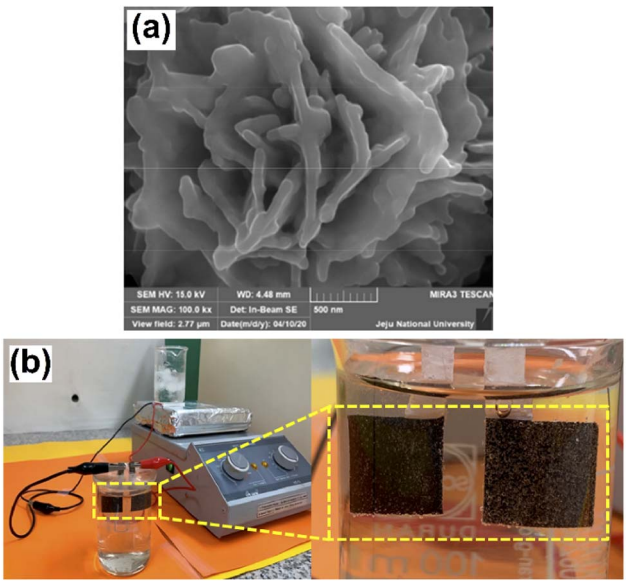

Fig. 7 (a) FE-SEM micrographs of the $CuFeS_2$ nanostructure obtained under various magnifications and (b) the real time application of thermoelectrically-driven self-powered water electrolyzer using $CuFeS_2$ as both the negative (cathode) and positive (anode) electrode in 1.0 M KOH electrolyte. Reproduced with permission from ref. 60. Copyright 2021 American Chemical Society.

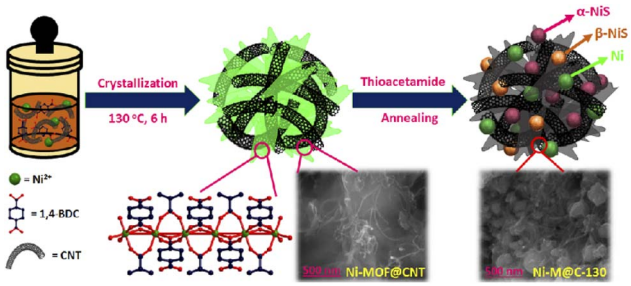

Fig. 8 The schematic Illustration of Ni/(α,β)-NiS heteronanoparticle-implanted semi-MOF nanosheets fabrication strategy and their morphological images. Reproduced with permission from ref. 61. Copyright 2021 American Chemical Society.

electrocatalyst (Fig. 8). The Ni/NiS electrocatalyst was considered as a potential electrode material for electrolysis in the WS reaction. The heterostructure nanoparticles possessed larger surface-to-volume ratio and required lower overpotential values for both OER (η = 244 mV) and HER (η = 123 mV) to produce sustainable H_2 energy.[61] Wu *et al.*[62] demonstrated the three-different morphological (nanosheet, nanoneedles, and nanoplate) Zn-Co mixed sulfide electrocatalysts that have been grown on carbon fiberpaper (CFP) by a hydrothermal technique, followed by the sulfuration method. The established nanostructured Zn-Co-S/CFP electrocatalyst exhibits an effective active surface area and can act as a promising material for WS reaction and metal–air battery applications.

5. Transition metal oxide-based electrocatalysts for green energy

Transition metal oxides (TMOs) have sparked scientific attention in both practical and fundamental science sectors, and they are a key component of the emerging field of quantum matter.[63] TMOs phases result from the complicated interaction of comparable energy scale interactions such as crystal-field splitting, electron–electron interaction, Hund's coupling, and spin-orbit coupling (SOC).[64,65] The B-site ion in TMOs is surrounded by O^{2-} ions, which generate the static electric field. The type of bonding between metal and oxygen can range from moderately ionic to very covalent (or metallic). TMO characteristics are remarkable due to their outer d-electron composition. The outstanding properties of TMOs are the remarkable range of electronic and magnetic characteristics. Consequently, oxides with metallic behavior such as RuO_2, $LaNiO_3$, and ReO_3 are classified as one class, whereas oxides demonstrating extremely insulating characteristics such as $BaTiO_3$ are classified as the other one.[66,67] TMOs vary in structure from cubic symmetry to triclinic, but MO_2-type composition includes rutile, fluorite, and distorted rutile (complex structure).[68] Its display a variety of features that make them suitable for catalytic applications, including the thermal and mechanical stability required to withstand severe reaction conditions. More significantly, transition metal cations can exist in numerous valence states. TiO_2 has a bulk band gap energy of about 3.2 eV, although vacuum annealing may deposit electrons in the (3d)

gap states about 0.7 eV below the Fermi level. In contrast, the d orbitals of the main group metal oxides such as MgO (bulk band gap *ca.* 7.7 eV) are not accessible.[69] TMOs are composed of oxygen atoms bonded by a central TM to create various lattices or crystal structures such as monoxide (NiO), dioxide (MnO_2), perovskite ($LaNiO_3$), and spinel ($NiCo_2O_4$). A partially filled d-valence of TM produces spin and orbital degrees of freedom, which enhances electron flow back and forth in the complex between free oxygen and TM, resulting in higher ORR activity.[70] Compared with all-TMOs, manganese oxides (MnO_x) have a long history of usage as an active electrochemical material in primary batteries, such as alkaline MnO_2 cells and zinc carbon cells.[71] Vanadium-based oxides, such as carbide and nitride catalysts, have demonstrated high ORR activity and are widely utilized in electrochemical systems.[72] TMOs in various oxidation states are being evaluated as possible supercapacitor materials. As typical TMOs, ruthenium oxide (RuO_2), manganese oxide (MnO_2), cerium oxide (CeO_2), vanadium pentoxide (V_2O_5), nickel oxide (NiO), and cobalt oxide (Co_2O_3) have been investigated as supercapacitor electrode materials.[73,74]

$SrIrO_3$, with the highest spin-charge conversion efficiency of the three TMOs (*i.e.*, IrO_2, $SrIrO_3$, and $SrRuO_3$), is thought to be a promising material. The spin-Hall angle, defined as the ratio of the spin current to the applied charge current $|j_s/j_c|$, is estimated to be in the range of 0.3–1.0, which is significantly greater than the spin-Hall angle in conventional heavy metals such as Pt/Co (0.013–0.13).[75] $SrRuO_3$ is a TMO having a structure similar to $SrIrO_3$. Owing to the 4d element Ru, it has also generated interest in studying its SHE. More recently, Ou *et al.* fabricated the Co/$SrRuO_3$ bilayers on Si substrates with a $SrTiO_3$ buffer layer. The reported spin-Hall angle was in the range of 0.1–0.3 for the full ambient temperature range based on the ST-FMR results (the conductivity was assumed to be $13 \times 10^5\ \Omega^{-1}\ m^{-1}$, and the spin transparency was assumed to be 1).[76] Because of its high spin-hall angle and low electrical resistivity IrO_2, a simple binary oxide with a rutile structure has piqued the attention of many researchers. To prevent oxidation, Bose *et al.*[77] made-up an IrO_2/Py bilayer on (001) and (110) TiO_2 substrates with a thin Ir passivation layer. According to the ST-FMR measurements, the spin-Hall angle of (001) IrO_2 was found to be approximately 0.65, which was an order of magnitude greater than the preceding values. Due to their tunable charge states and stable structures, TMOs with abundant supplies and inexpensive prices have long been used in various catalytic processes. The properties of TMOs can be considerably affected by the surface oxygen vacancies. He *et al.*[78] used a lattice-refining technique to create a series of oxygen vacancy-abundant TMOs with high SSA. This technique uses urea-assisted ball-milling pyrolysis and is environment-friendly, efficient, and common. In a sample synthesis, TMOs and urea of a certain molar ratio were combined in a ball milling container and transported to a planetary ball mill with a 400 rpm rotation speed for 3 h. A stainless tank and 3 mm diameter zirconia balls were employed. The white mixture was then calcined at 900 °C for 2 h at a heating rate of 5 °C min^{-1} in a low-flow N_2 environment. A gray powder was obtained for further characterization after being naturally cooled to room temperature (Fig. 9).

The decrease of different kinds of Ti species corresponds to the H_2 uptake peaks at different temperatures. The reduction of Ti species peaks changed from 715 °C for D-TiO_2 to 521 °C for A-TiO_2, indicating that A-TiO_2 is more reducible. The existence of oxygen vacancies is accompanied by a significant number of Ti^{3+} metal sites that considerably improved the catalyst's

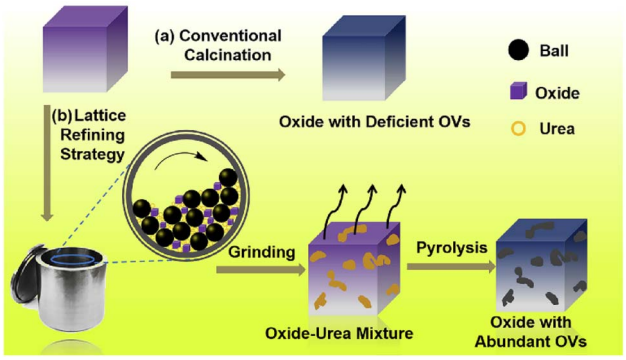

Fig. 9 Schematic illustration for the preparation process of TMOs with abundant OVs. Reproduced with permission from ref. 78. Copyright 2019 American Chemical Society.

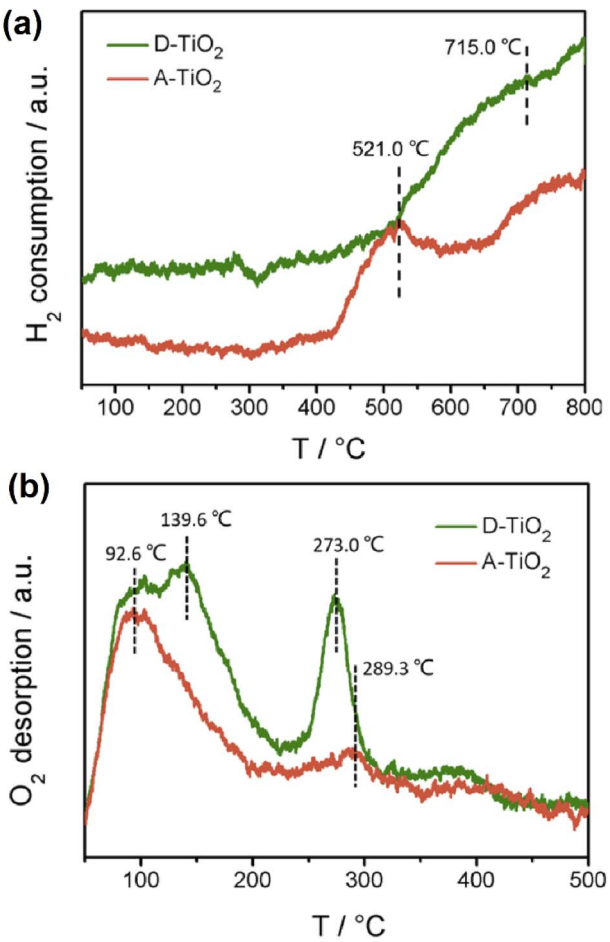

Fig. 10 (a) H_2-TPR profiles of A-TiO_2 and D-TiO_2, (b) O_2-TPD profiles of A-TiO_2 and D-TiO_2. Reproduced with permission from ref. 78. Copyright 2019 American Chemical Society.

reducibility. The chemisorbed O_2^- and O^- species, which are weakly associated with oxide defects, are assigned to the O_2 desorption peaks at 92.6 °C, as illustrated in Fig. 10.

Furthermore, the oxygen desorption temperature (92.6 °C) of A-TiO_2 was lower than that of D-TiO_2 (139.6 °C), indicating that the binding capacity between the chemisorbed oxygen species and the surface defect structures of A-TiO_2 was less. As the interaction between the chemisorbed oxygen species and the catalyst surface is weaker, it is simpler to dissociate, thus improving the oxygen mobility. This widespread viable design introduces novel ways for optimizing the oxygen vacancy structure, specific surface area, and surface disorder layer in TMOs for catalytic applications.[78] Romero *et al.*[79] investigated the usage of TMOs and Mo-based nanolayers to enhance the back interface of $Cu_2ZnSnSe_4$, Cu_2ZnSnS_4, and $Cu_2ZnSn(S,Se)_4$ solar cells made up on transparent glass/FTO substrates. As a result, record efficiencies of 6.1%, 6.2%, and 7.9% were attained for $Cu_2ZnSnSe_4$, Cu_2ZnSnS_4, and $Cu_2ZnSn(S,Se)_4$ devices, respectively, demonstrating the potential of TMOs for the development of kesterite solar cells on transparent substrates. Layered TMO-based on Mn and Fe should be the best cathode candidates for low-cost sodium batteries.[80]

6. Noble metal oxide-based electrocatalyst

One of the most recent approaches in the design of effective catalysts is the development of Pt- and Pd-based electrocatalysts. These catalysts are unique with many interesting properties such as defects due to long-range disordered lattice, defects-created low-coordination active sites, which have been reported to increase the catalytic activity.[81,82] In addition, the synergistic effects of doping and alloying elements also contribute to higher catalytic activity.

In recent years, Pt- and Pd-based alloys including Pt–Ru, Pt–Sn, Pt–Pd, Pd–Co, Pd–Au, Pt–Ru–Mo, and Pt–Ru–Ni have shown significant higher electrocatalytic activity in both acidic and alkaline media compared to pure noble metal catalysts.[83,84] Xu and coworkers[85] developed a coordination polymer nanosheet-engaged approach to fabricate porous mono Pd nanosheets *via* sequential topotactic conversions. Pre-synthesized Hofmann-type coordination polymer square nanosheets were converted into bimetallic Pd–Ni oxide *via* calcination and eventually transformed into porous mono Pd nanosheets (Fig. 11a). Benefitting from their highly porous structure, the porous nanosheets could provide a high density of surface Pd atoms, more electron transfer, and rich mass diffusion channels. As a result, such Pd porous nanosheets could display extraordinary electrocatalytic performance toward the electrooxidation of alcohol and ORR (Fig. 11b).

This unique feature is advantageous in developing bimetallic structure with single crystallinity, which facilitates the electrocatalytic activity *via* the coupling effect.[86] Moreover, the selection of suitable supportive materials and control of catalyst dispersion on the support play an essential role on the activity of the catalyst.

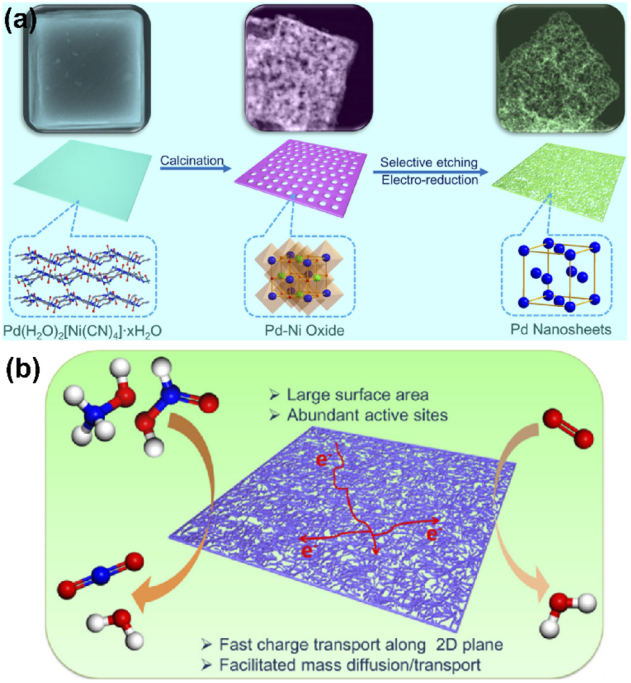

Fig. 11 (a) Schematic illustrations of the synthesis process of porous Pd square nanosheets and (b) schematic demonstration of the structural advantages of porous Pd square nanosheets as advanced bifunctional electrocatalysts for FOR and ORR. Reproduced with permission from ref. 85. Copyright 2019, Elsevier.

Carbon nanomaterials are gaining extensive attention in the fabrication of electrocatalysts with Pt–Pd, in which the synergetic effect between the metal and the support is vital, which endows enhanced catalytic performance and long-term durability.[87] Arukula *et al.*[88] synthesized the rGO/PANI/Pt–Pd composite *via* a wet reflux strategy. The prepared composite was extensively characterized. The cumulative effect of Pt–Pd, PANI,

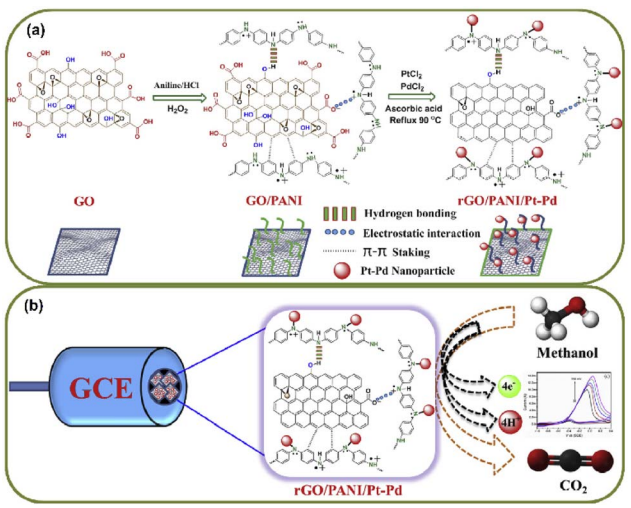

Fig. 12 Schematic illustration of (a) the preparation of rGO/PANI/Pt–Pd and (b) the electrocatalytic oxidation of methanol on rGO/PANI/Pt–Pd. Reproduced with permission from ref. 88. Copyright 2019 Elsevier Publications.

and rGO in the enhancement of methanol oxidation activity was also scrutinized. The electrocatalyst exhibits a special geometric configuration of bimetallic alloy in rGO/PANI layers that suppresses the agglomeration of the alloy and promotes the electrooxidation of methanol. The key parameter of the rGO/PANI/Pt–Pd composite is the successful interfacing of PANI between rGO and Pt–Pd, which improves the synergistic/electronic effect between the rGO and Pt–Pd. Besides, PANI assists water absorption on the catalyst and promotes CO oxidation to CO_2, thereby reducing the poisoning of the catalyst. The effect of combination of the carbon support, conductive polymer, and bimetallic alloy on DMFC performance through morphological, structural, and electrochemical properties has been reported. Fig. 12a and b illustrates the scheme of preparation of rGO/PANI/Pt–Pd.

The anode catalyst's capacity to oxidize methanol is a significant element that directly affects the DMFC's final power efficiency. Eqn (1)–(3) provide the commonly recognized standard chemical steps for electrooxidizing methanol with a Pt-based catalyst.[89] In eqn (1), CO was produced as a result of methanol electrooxidation and this intermediate was further adsorbed onto the Pt–Pd surface as Pt–Pd-CO_{ad}. This CO_{ad} blocks the Pt–Pd surface, thereby suppressing continuous methanol oxidation. In eqn (3), the CO adsorbed on the Pt–Pd surface could be oxidized to CO_2 by OH. The Pt–Pd catalyst was supported by rGO/PANI, which prolongs the catalyst's life by preventing nanoparticle aggregation during the reaction.

$$PtPd + CH_3OH_{bulk} \rightarrow PtPd\text{-}CO_{ad} + 4H^+ + 4e^- \quad (1)$$

$$PtPd + H_2O \rightarrow PtPd\text{-}OH_{ad} + H^+ + e^- \quad (2)$$

$$PtPd\text{-}CO_{ad} + PtPd\text{-}OH_{ad} \rightarrow CO_2 + 2PtPd + H^+ + e^- \quad (3)$$

The successful interface of PANI between rGO and Pt–Pd, which enhances the synergistic/electronic impact of the catalyst, is the main component of the rGO/PANI/Pt–Pd composite. This unique geometric design successfully prevents alloy agglomeration and enhances the electrochemical stability.

The synergetic effect is mainly determined by the following three kinds of effects: (i) the ligand effect: the different composition of the core and shell leads to electron transfer and a change in the band structure; (ii) the strain effect: the tension or compression of the noble metal shell lattice causes a change in the surface adsorption energy; (iii) the geometric effect: the different three-dimensional structure of the surface atoms can affect the electrochemical properties.[90] Through the combination of these effects and theoretical calculation, core–shell structured noble metal-based nanomaterials with better ORR properties can be reasonably designed and prepared.[91]

7. Rare earth metal oxide-based electrocatalyst

Most commonly, rare earth metal oxide-based materials have been proved as promising and efficient electrocatalysts for electrochemical applications owing to their unique physical/chemical properties and also their diverse applications. This type of heterostructured materials containing both metal oxides could be beneficial for achieving desired bifunctional activities toward the electrochemical reactions.[92,93] Hussein *et al.* discussed the recent literature on rare earth metal oxide-based materials, various synthesis approaches, and characterization through different analytical and electroanalytical technique to estimate their electrocatalytic activities.[94] Ilanchezhiyan *et al.*[95] prepared a highly-efficient bifunctional Gd_2O_3-In_2O_3-ZnO ternary oxide by a simple hydrothermal process. The ternary oxides demonstrated superior HER and OER activities under basic conditions, with the reported overpotential (η) values of 271 and 282 mV at $\pm$10 mA cm^{-2}, respectively. An interesting monoatomic Ru-supported CoFe-based layered double hydroxide (LDH) was prepared by the solid gray precipitant technique (Fig. 13a). The clean surface of the morphological nanosheet-based Ru-CoFe LDHs was analyzed through thHAADF-STEM images, wherein the corresponding element distribution (Ru, Ni, and Fe) could possess a strong electrostatic interaction between Ru and CoFe LDHs (Fig. 13b). The Ru-CoFe LDHs heterocatalyst displayed outstanding electrocatalytic activity for OER with an overpotential of 198 mV and an applied current density of 10 mA cm^{-2} (Fig. 13c).[96]

Currently, great effort has been made for the development of multifunctional-based Ru, Co-embedded nitrogen-doped carbon (RuO_2/Co_3O_4-RuCo@NC) matrix by a sacrificial template (Fig. 7a), which was used as a Mott–Schottky electrocatalyst. The highly crystalline distinguishable lattice frings were clearly observed from the HR-TEM images (Fig. 14b). Subsequently, the as-prepared RuO_2/Co_3O_4-RuCo@NC Mott–Schottky matrix exhibited better electrocatalytic activities toward OER/HER studies under highly acidic conditions with affordable overpotentials of 247 and 141 mV, respectively (Fig. 14c).[97]

Wu *et al.*[98] designed CeO_x-decorated hollow-structured $NiCo_2S_4$ tubular arrays (CeO_x/$NiCo_2S_4$) by the self-assembly

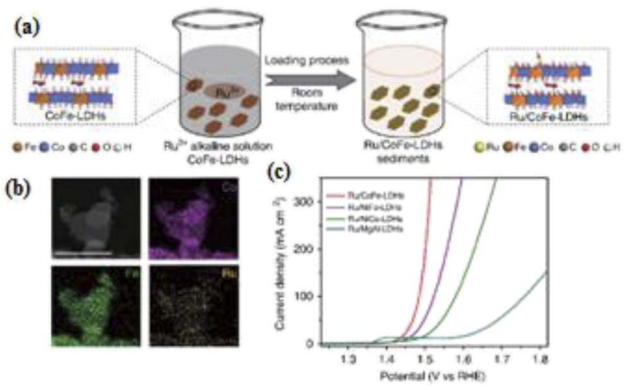

Fig. 13 (a) Schematic illustration of the hydrolysis-deposition to form Ru/CoFe-LDHs, (b) the HAADF-STEM images of the Ru/CoFe-LDHs and corresponding elemental distribution maps of Ni, Fe, and Ru in the Ru/CoFe-LDHs. Scale bar: 50 nm, and (c) the comparison of OER overpotentials and Ru contents in different catalysts at a current density of 10 mA cm^{-2}. Reproduced with permission from ref. 96. Copyright 2019 Springer Nature.

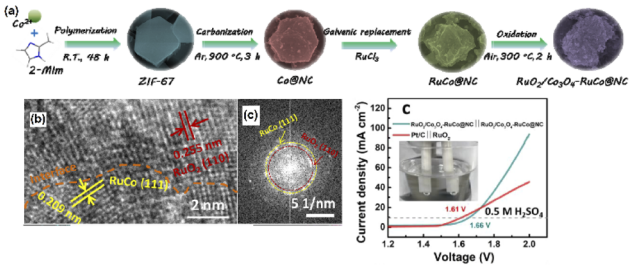

Fig. 14 (a) Schematic illustration of the synthesis process of RuO_2/Co_3O_4-RuCo@NC, (b) enlarged HRTEM images and FFT patterns in section I and section II, and (c) the polarization curves for overall WS in 0.5 M H_2SO_4. Reproduced with permission from ref. 97. Copyright 2019 American Chemical Society.

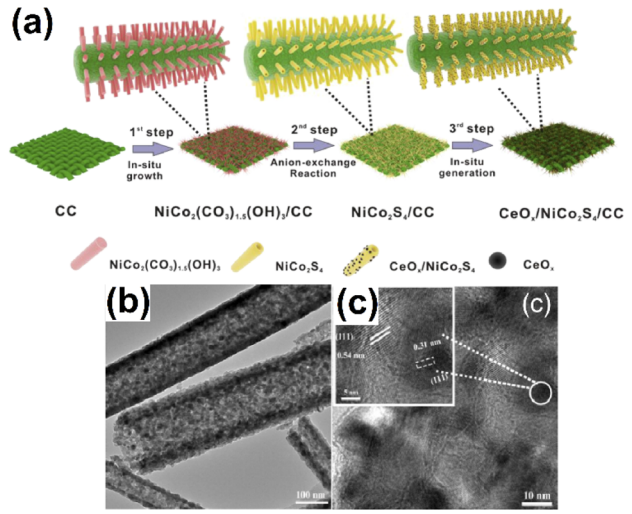

Fig. 15 (a) Schematic illustration of the formation of CeO_x/$NiCo_2S_4$/CC, (b) TEM images of CeO_x/$NiCo_2S_4$/CC, and (c) HRTEM image of CeO_x/$NiCo_2S_4$/CC. Reproduced with permission from ref. 98. Copyright 2019 American Chemical Society.

method (Fig. 15a). The typical tubular morphology the CeO_x/$NiCo_2S_4$ electrode surface and their surface roughness was distinctly observed from the TEM analysis (Fig. 15b). The proposed CeO_x/$NiCo_2S_4$ electrocatalyst greatly enhanced their OER activities with favorable potential values of 270 mV. Sun and his co-workers decorated the cerium-based iridium oxide-supported α-MnO_2 (Ce-Ir-O_x/Mn) hybrid catalyst through the two-step hydrothermal process. The assembled hybrid catalyst has gained much attention due to the significant enhancement of the OER activity.[99]

8. Polymer hybrid-based electrocatalyst

A composite material is one that contains at least two physically or chemically distinct, correctly organized, or dispersed phases separated by an interface. Technological advances necessitate materials with a unique matrix of characteristics that standard materials cannot provide.[100] Fiber-reinforced polymer composites have been widely employed in the aerospace, car, marine, and military sectors in recent years due to their superior mechanical and electrical properties.[101] Nevertheless, the advantages of these materials are significantly decreased due to their possibility to fracture in low-velocity collisions.[102] A hybridization procedure improves the characteristics of the composite materials. The combination of many composite types into a unified framework has resulted in the development of hybrid composites.[103] Nanocomposites are a fundamentally distinct type of composites, in which at least one component has nanometer scale dimensions (1–100 nm). Polymeric nanocomposites have demonstrated significant gains in mechanical parameters such as strength and stiffness without altering the density, toughness, or processability. The increased surface area-to-volume ratio of the nanostructured material as compared to the conventional material accounts for significant performance difference between nanocomposites and conventional materials. Nanostructured materials can have substantially different characteristics than larger dimension materials because the surface controls numerous critical physical and chemical interactions. In fibers, the diameter of the fiber and surface area per unit volume were inversely proportional to each other. The aspect ratio of the nanomaterial impacts the efficacy of reinforcing.[104] *In situ* polymerization, solution, and melt blending are the three different approaches that may be used to manufacture polymer hybrid nanocomposites. However, only two of the aforementioned processes, solution and melt blending, are used to create hybrid nanocomposites based on polyolefin matrices, with the latter way accounting for a great majority.[105] Depending on the kind of nanofillers, the insertion of a hybrid system of nanofillers into the polymer matrix was done to give nanocomposites with appropriate mechanical, thermal, optical, barrier, or biological characteristics. The size and shape of nanofiller particles, specific surface area, surface development, surface energy, and the dispersion of nanoparticles in the polymer matrix lead to a considerable improvement in the polymer nanocomposites' characteristics.[106] The size of the particles, the quality of the dispersion, interfacial interactions, and the concentration of nanoparticles influence the mechanical properties of polymer hybrid nanocomposites.[107] The impact of U-irradiation on the mechanical characteristics of titanium-oxide nanoparticles (TiO_2NPs)/MWCNTs hybrid LDPE-based nanocomposites was explored by Zagho *et al.* The authors used the melt-mixing procedure to make an LDPE hybrid nanocomposite, which then subjected the samples to various dosages of U-radiation (5 to 50 kGy). They discovered that after adding TiO_2NP or MWCNT, the tensile strength first reduced but then increased along with a rise in the MWCNTs' concentration. They also observed the effect of U-radiation at doses of 2 and 5 kGy on the tensile strength of the nanocomposites. They found that exposing composites to a dose of U-radiation resulted in a decrease in their tensile properties.[108] Polymer/metal oxide nanocomposites have a lot of potential since they can provide the required stability and processability while also having unique optical features. *In situ* polymerization was used to synthesize the transparent ZnO/epoxy nanocomposites. The optical properties of the

synthesized samples were studied, and it was discovered that they were dependent on the particle size and ZnO content. After calcination at 350 °C, very little (0.07 wt%) ZnO NPs with an average particle size of 26.7 nm was detected, which had great visible-light transparency and UV-light shielding efficiency, making it more suited to a variety of important applications.[109] The temperature-dependent luminescence feature of the nanocomposites ($NaGdF_4$: Er, Yb@UiO-66-NH_2, $NaGdF_4$: Tm, Yb@UiO-66-NH_2, and $NaYF_4$: Er, Yb@$NaYF_4$@UiO-66-NH_2) is exceptional. These nanocomposite materials can be used as a catalyst for the esterification of acid with methanol to produce methyl laurate. The $NaGdF_4$/$NaYF_4$ nanoparticles in MOF had no effect on the catalytic performance of the catalyst.[110] Owing of their superior electrical, mechanical, and gas-barrier capabilities, graphene-based polymer nanocomposites have attracted great interest from the polymer and nanomaterial sectors in recent years. Hou *et al.*[111] described a facile yet adaptable approach for reducing graphene oxide (GO) and polymerizing styrene at the same time to make reduced graphene oxide/poly(styrene) (RGO/PS) nanocomposite materials by microwave heating (Fig. 16a). By vacuum pressing powdered samples at 105 °C for 10 min, the RGO/PS nanocomposite materials were processed into films of specified thicknesses. The inclusion of a higher dielectric constant filler into the polymer matrix resulted in the RGO/PS polymer nanocomposites having higher static dielectric constants than pristine PS (Fig. 16b).

The simultaneous reduction/polymerization technique described here might be used to make it easier to make and treat dielectric materials for energy storage. Wang *et al.*[112] describe a photosensitizer-loaded hybrid nanostructure with strong antibacterial efficacy upon surface contact with a lectin protein. An *in situ* reduction approach was used to create gold nanoparticles on the polymer nanoparticle surface. The as-prepared nanostructure significantly improved the antibacterial efficacy of ROS (reactive oxygen species) and provides an alternate technique for controlled antibacterial testing.

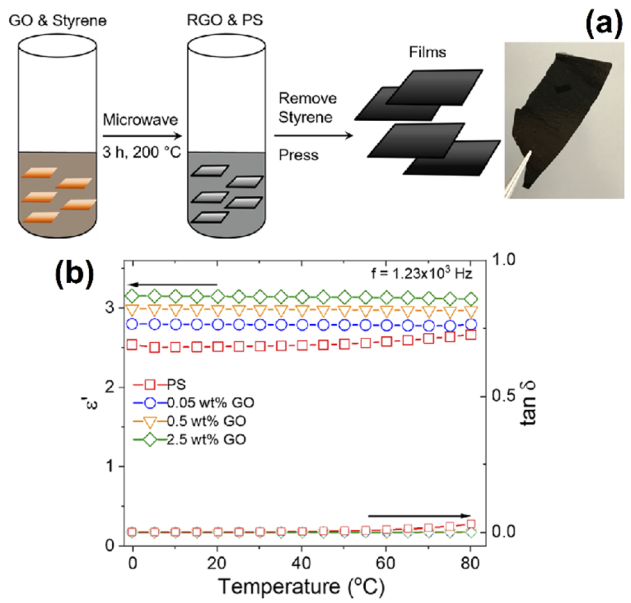

Fig. 16 (a) Overview of the synthetic and processing method for the preparation of RGO/PS polymer nanocomposites (b) temperature dependence on the static dielectric constant and tan δ of RGO/PS nanocomposite materials. Reproduced with permission from ref. 111. Copyright 2020 American Chemical Society.

9. MXenes based-electrocatalyst

A budding family of MXenes, *i.e.*, layered transition metal carbides and/or nitrides, has become an important catalytic material toward energy storage and conversion devices due to their exceptional properties.[113] Recently, the MXene family has been employed in energy storage devices, mainly ion batteries, supercapacitors, ion capacitors, H_2 storage systems, conversion devices such as fuel cells and its associated devices, namely, H_2 generation and O_2 evolution. The relationship between the electrochemical performance and the structure has been deeply explored.[114] Two-dimensional (2D) materials have attracted increasing attention due to their notable physical/chemical properties as compared with their bulk counterparts. As a frequently-discussed 2D material, graphene has been regarded as a potential candidate in a wide range of applications. In the recent past, information regarding the design of MXene-based nanocomposites with interesting activities for excellent oxygen evolution reaction (OER) and ORR are still at an early research stage because of their slow kinetics. In this view, we predict that these informations will lead to a decent framework to encourage interest in the pursuit of engineering and science toward MXene composites for potential OER and ORR applications in the field of clean energy conversion.[115] These studies validate the clear role of MXenes-2D-based substrate incorporated with other active catalyst materials to design resourceful MXene-based composite heterostructures with micro/nanointerfacial electrocatalysts.[116]

The pure MXene displayed nearly no ORR activity because of the absence of active locations for the generation of oxygen. However, Fe–N–C electrocatalysts offer a promising alternative for noble metal catalyst. Zhao *et al.*[117] reported the Fe–N–C-supported Ti_3-C_2-based MXene. It was appealing to note that Fe–N–C@Ti_3-C_2 MXene showed an incredible increase in the electrocatalytic activity of ORR with a half-wave potential of 0.777 V and a limited current density of 5.7 mA cm^{-2} in acidic medium.

Recently, photocatalytic H_2 production has found extensive interest. Chandra's group developed a Ti_3C_2-based MXene-supported CdZnS composite for photo and electrocatalytic H_2 generation. In the photochemical reaction, H_2 was generated at the rate of 15 035 μ mol g^{-1} h^{-1}. In addition to that, the transition metal doping enhanced the H_2 generation rate to 17 070 μ mol g^{-1} h^{-1}. Thus, doping and the 2D design of the catalyst increase the light adsorption at low photon flux density and help to trap the electrons in the ultrathin layers.[118]

Compared to single metal, recently, double metal-based MXenes have found extensive interest. Geng *et al.*[119] designed a catalyst and with the help of DFT studies found that Cr_2-TiC_2S_2, $Cr_2ViC_2S_2$, and $Mo_2TiC_2S_2$ are active catalyst, while the low Gibbs free energy makes the materials promising

candidates toward the H_2 evolution reaction. In addition, these catalysts showed a superior magnetic property and were proposed as promising materials for magnetic nanodevices. In a recent study by Thirumal *et al.*,[120] they developed a 2D heterostructured graphene and MXene-based catalyst prepared by hydrothermal methods, which resulted in an overpotential value of 121 mV toward HER because 2D structured graphene can increase the conductivity and active platform, giving a better electrocatalytic response.

Titanium-based MXene-$Ti_3C_2T_x$ was developed by Geng *et al.* based on facile flash oxidation at 200–900 °C for 1 to 3 min,[121] which led to decreased band gap energy extended absorption of light in the visible region. The catalyst was tested for the photocatalytic degradation of methylene blue dye. In addition, due to the low imaginary permittivity and dielectric loss, the material exhibited good microwave transparent performance. It can a potential candidate for photocatalytic H_2 generation. Cui *et al.*[122] developed a novel type of two-dimensional MXene-supported bimetallic oxide alloy ($PtO_aPdO_bNPs@Ti_3C_2T_x$) electrocatalyst *via* the solution plasma technique (Fig. 17a). The as-prepared $PtO_aPdO_bNPs@Ti_3C_2T_x$ catalyst could serve as a promising candidate for water electrolysis applications. Further, the MXene electrocatalyst was tested for long-term stability through the chronoamperometry method (Fig. 17b).

The sheet-like as well as nanobelt-based $Ti_3C_2@MoO_3$ nanocomposite was prepared by the hydrothermal method.

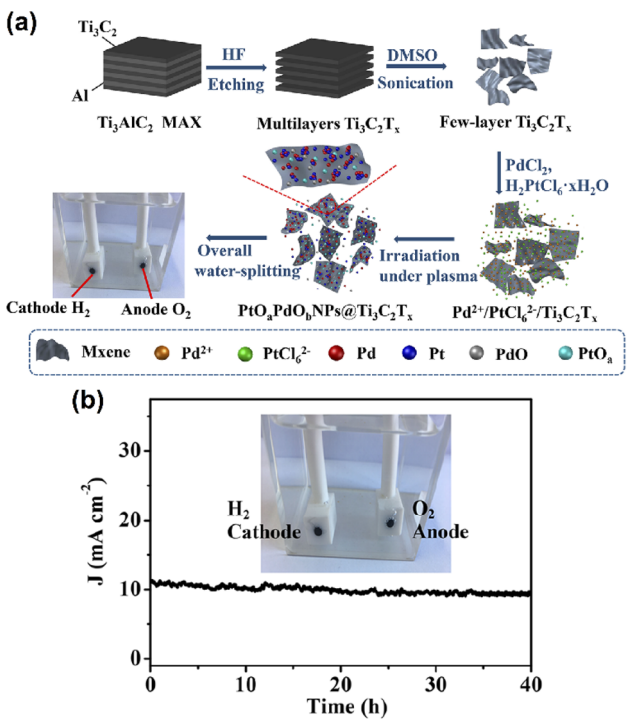

Fig. 17 (a) Schematic diagram of the preparation of PtO_aPdO_b-$NPs@Ti_3C_2T_x$ nanosheets by the SP method and its application as an electrocatalyst for WS and (b) long-term durability test of the PtO_a-$PdO_bNPs@Ti_3C_2T_x$ electrolyzer at 10 mA cm^{-2} (200 W, 3 min) and the photograph during the overall WS (the inset). Reproduced with permission from ref. 122. Copyright 2018 American Chemical Society.

Thus, there was a strong electronic coupling between Ti_3C_2 and MoO_3, which could accelerated their electrocatalytic activity in WS reactions. The developed $Ti_3C_2@MoO_3$ could play the crucial role in both HER and OER activity.[123] On the other hand, Thirumal *et al.*[124] reported a novel 2D transition metal carbide-based MXene ($MX = Ti_xC_xT_x$) (MX@Pt) nanocomposite that can enable HER studies, which displayed a potential of 165 mV@10 mA cm^{-2} and also exhibited 477 mV@100 mA cm^{-2}.

As a large volume of reports indicates, titanium-based MXene catalysts have undergone extensive study in both electrochemical and photochemical systems toward fuel cell applications. Also, the addition of heterostructures and carbon supports enhance the H_2 generation. However, there are still several undiscovered catalysts with potential applications, And both theoretical and experimental studies are essential to unearth them.

10. Multimetallic electrocatalysts

In recent years, precious metals have become prominent candidates in electrochemical applications; however, their high cost, wider pH ranges, and scarcity restrict their practical applications.[125] Accordingly, multifunctional active sites-based electrocatalysts are the key that enable their electrode surface curvature and enhance their electrocatalytic activities toward OER.[126] The N-engineering ultrathin bimetallic nanosheet multifunctional electrocatalyst has been widely used as a new catalyst for the study of the WS process, which is mainly due to its low cost, controllable valence state, and greatly enhanced catalytic activities.[127] Similarly, the heterostructured Ni–Fe–Co (NFC)-based metal oxide was encapsulated on carbon nanosheets (CNSs) *in situ*, followed by simple pyrolysis methods. The derived NFC@CNSs electrocatalyst has enhanced textural properties, increased porosity, and surface area and structure control, which enhance its electrocatalytic performance.[128] An interesting bicontinuous nanoporous structure of NiFeCoP-bifunctional electrocatalyst was prepared by a new type of melt-spinning technique. This type of NiFeCoP ternary array could improve the electrocatalytic activities due to increasing surface modification process and higher active sites, which exhibit a positive effect on the electrocatalytic behavior.[129] Among these electrocatalysts, the hierarchical nickel-iron nanosheets were directly developed on macroporous nickel foam by the electrodeposition method. The developed three-dimensional Ni–Fe-based composite showed great promise as an active electrocatalyst for large-scale industrial application of WS reactions, with a reported overpotential value of 200 mV@500 mA cm^{-2}.[130] The salient feature is the well-defied ultrathin nanosheet morphological structure of the trimetallic Co–Ni–Ru–S–Se nanocomposite matrix, which was used as an important benchmark for OER catalytic activity under alkaline conditions.[131] One of the most effective approaches was used for the fabrication of a multifunctional (CoNi-N-CNT) electrocatalyst owing to its tunable atomic structure and three different active sites, for example, N-doped CNT, Ni–N–C, and CoNi alloys, respectively. These types of active sites could contribute synergetic catalytic performance in sustainable as

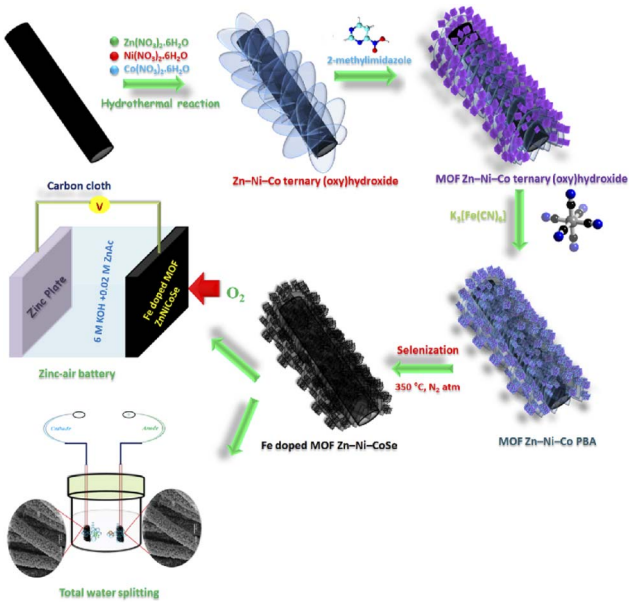

Fig. 18 Schematic diagram for the Fe-doped MOF ZnNiCoSe@CC synthetic strategy and electrochemical applications. Reproduced with permission from ref. 133. Copyright 2020 American Chemical Society.

well as clean energy technology.[132] Alagan Muthurasu and coworkers[133] constructed Fe-doped MOF-derived ZnNiCoSe on carbon cloth (CC) by a facile hydrothermal technique (Fig. 18). The constructed Fe-doped MOF ZnNiCoSe@CC electrocatalyst, which acts as both the anode and cathode, significantly enhanced the WS process. In this respect, they delivered high capacity, increased power density, as well as excellent cyclic (charge–discharge) stability. Similarly, the hierarchical $CuCo_2O_4$@carbon quantum dots (CQDs) hollow microspheres-based electrode was successfully constructed through the hydrothermal route. The well defined hollow $CuCo_2O_4$@CQDs facilitated desirable electrochemical performance owing to its potential synergetic effect in both OER and HER in alkaline conditions.[134]

Wang *et al.*[135] constructed a $PtSe_2$/Pt-based heterointerface, achieving their thermoneutral free energy change and extraordinary HER activity with a resulting overpotential of 42 mV@10 mA cm^{-2} under acidic conditions. The self-reactivated platinum-based thorium oxide-supported carbon (Pt-ThO_2/C) composite was assembled hydrothermally, followed by the electrochemical deposition technique. The as-prepared Pt-ThO_2/C catalyst was applied in direct ethanol fuel cell and displayed maximum power density.[136] Lu *et al.*[137] overviewed the electrochemical impacts of ligands on heterogeneous electrocatalysts, which is the vital role of ligands in the synthesis of heterogeneous-based electrocatalyst to control their size and shapes. Mainly, the ligand surface was calculated through density functional theory (DFT) and also well explained the ligand-promotion mechanism for the nanocatalyst. Ruthenium-based electrode materials have received much interest because of their good electrochemical properties. Lu *et al.*[138] used a novel nanowire morphological ruthenium and nitrogen co-doped (RuC_xN_x) electrocatalyst by the hydrothermal route. For instance, this RuC_xN_x material has been considered as a fascinating material for HER, having the most catalytically active centers and reaching an effective current density of 10 mA cm^{-2} in alkaline conditions. Interestingly, ultrasmall Ru_2P@Ru/CNT multiinterface heterojunction nanocatalyst was synthesized using the solvent-free microwave technique. Notably, the optimized ratio of the Ru_2P@Ru/CNT electrode materials exhibited excellent electrical conductivity and was explored as a promising candidate for boosting the HER activities in alkaline conditions as well as real sea water analysis.[139] Similarly, Wu *et al.*[140] used a fast, simple and solvent-free pyrolysis technique for the preparation of ultrasmall particle Ru-MO_2C@CNT electrocatalyst, which had the highest reached current densities of 10 mA cm^{-2} with a turnover frequency of 21.9 S^{-1} in 1.0 M KOH medium. Consequently, a Cu-doped Ni catalyst modified with Ni-O-VO_x site using the electrodeposition technique, wherein the fabricated Ni(Cu)VO_x composite created an excellent electrocatalytic active surface area, could be used for the study of industrial alkaline-based water electrolysis.[141] This type of ultrathin nanosheet morphological RuPdNi electrocatalyst was prepared by wet-chemical approaches, which are were found to be 9.6 times better than the than that of Pt/C and Pd/C electrocatalysts.[142] Zhang *et al.*[143] used a multisite-based PdFeCoNiCu/C electrocatalyst by a facile oil-phase method. The fabricated PdFeCoNiCu/C electrocatalyst showed excellent alkaline HER activities with a reported overpotential of 18 mV and Tafel slope of 39 mV dec^{-1}. Nanoporous three-dimensional Pt-Ag-Al electrocatalyst was prepared through a facile and scalable alloying/dealloying process, which generally offered high density and good active sites and was a promising alternative to Pt catalyst for highly efficient H_2 production.[144] Wang *et al.*[145] used a solvent-free and superfast strategy for the production of refractory ultrafine Pt-lanthanide-based Ketjen black (PtM@KB) composite, which delivered an excellent electrocatalyst for HER with a lower overpotential of 38 mV with good cyclic stability (500 h). Zhang *et al.*[146] prepared a cost-effective novel opal-like MoxC(α-MoC_{1-x}/β-Mo_2C) nanosphere electrocatalyst by a facile strategy. In particular, the optimized composite demonstrated superior HER activity under acidic conditions with a small Tafel slope value of 48 mv dec^{-1} and remarkable cyclic durability. Similarly, the uniformly distributed unique N,P and N,S dual-doped MoC/C hybrid electrocatalyst was obtained by a facile two-step pathway. The designed dual-doped NP-Mo_2C/NS-Mo_2C exhibited lower resistance, excellent intrinsic activity and good electrochemical performance in HER activity with good electrode stability in acidic conditions.[147] The unique ultrafine morphological tungsten phosphide (WP) electrocatalyst could be used for the HER study due to its unique catalytic activity, excellent electronic properties, and superior electrocatalytic activity with a small Tafel slope of 52 mV dec^{-1}.[148] For the first time, simultaneous phosphorization and carbonization processes for the fabrication of α-molybdenum carbide and molybdenum phosphide-based heterostructured modified in N-doped carbon (α-MoC_{1-x}-MoP/C) matrix led to an excellent HER activity with the reported Tafel slope of 57 mV dec^{-1}.[149] The large surface area-based porous architecture molybdenum carbide-embedded N,K Co-activated

biochar (Mo_2C/NKAB) electrocatalyst was prepared by a scalable method. As a result, the optimized Mo_2C/NKAB electrocatalyst promoted higher intrinsic activity toward efficient HER.[150] Zhang *et al.*[151] developed a high performance ultrafine W_2C nanoisland monodispersed N,P dual doped carbon framework that could be used as an effective electrocatalyst for both acidic as well as alkaline HER. A new strategy was employed to design sulphur-substituted molybdenum carbide (S-MoC) electrocatalyst as one of the promising electrocatalyst for HER studies due to their d-band electronic structures with zero H_2 adsorption energy.[152,153]

11. Conclusions

H_2 fuel cells have been produced through different electrolysis routes, and have become a larger share of the global energy storage device market due to their high flexibility and eco-friendly nature. Several novel fabricated electrocatalysts have also been highlighted, and their electrocatalytic activity has been discussed, paving the way to the commercialization process. Notably, functionalized derived active materials can also be used as catalysts, which could assist in the electrochemical mechanism to improve the electrochemical performances with their fuel cell efficiencies under both acid as well as alkaline conditions. H_2 produced *via* water electrolysis can act as an ideal clean chemical fuel with superb gravimetric energy density and high energy conversion efficiency, solving the problems of conventional fossil fuel exhaustion and environmental contamination. Most importantly, an easy fabrication approach can design a stable electrocatalysts, which can allow faster electron transport process, thus making them greatly important for next-generation fuel cell devices. H_2 fuel cells could play an important complementary role for the production of electricity and also focused planning for the stakeholders in industry, investors, and government sectors. Recently, several efforts have been made in the successful development of H_2 fuel cell vehicles (FCV) to build a worldwide H_2 refueling network station for the launching of the FCV market.[154,155] One of the most promising high active metal oxide-based electrocatalyst has been used as a significant one to achieve the fascinating WS reaction with boosted electrocatalytic activities. Next, transition metal sulfides (TMS) have also been extensively explored as effective, widely available alternatives to precious metals in the overall WS process due to their physicochemical properties with well-defined nanostructures, controllable compositions, and excellent performance. Importantly, the intrinsic activities of electrocatalysts and several strategies for improving their bifunctional electrocatalytic performance during water electrolysis have been reported. Moreover, the design and fabrication of nanostructed bifunctional electrocatalysts with excellent performance can accelerate their large-scale practical application in water electrolysis.

Conflicts of interest

There are no conflicts to declare.

Acknowledgements

The financial support (MOST 107-2113-M-027-005-MY3 and MOST 111-2113-M-027-002 to SMC) from the Ministry of Science and Technology (MOST), Taiwan is applicated. R.R. thanks the Science and Engineering Research Board (SERB, File No. EEQ/2016/000427) New Delhi, India, for the financial support.

References

1 B. M. Hunter, H. B. Gray and A. M. Muller, *Chem. Rev.*, 2016, **116**, 14120–14136.
2 L. Dai, Y. Xue, L. Qu, H. J. Choi and J. B. Baek, *Chem. Rev.*, 2015, **115**, 4823–4892.
3 G. P. Peters, R. M. Andrew, J. G. Canadell, P. Friedlingstein, R. B. Jackson, J. I. Korshakken, C. Le Quere and A. Peregon, *Nat. Clim. Change*, 2020, **10**, 3–6.
4 Y. Devrim, S. Erkan, N. Bac and I. Eroglu, *Int. J. Hydrogen Energy*, 2012, **37**, 16748–16758.
5 A. Ehsani, M. G. Mahjani, F. Babaei and H. Mostaanzadeh, *RSC Adv.*, 2015, **5**, 30394–30404.
6 Y. Zhou, C. H. Wang, W. Lu and L. Dai, *Adv. Mater.*, 2020, **32**, 1902779.
7 J. A. Turner, *Science*, 2004, **305**, 972–974.
8 B. C. H. Steele and A. Heinzel, *Nature*, 2001, **414**, 345–352.
9 I. V. Pushkareva, A. S. Pushkarev, S. A. Grigoriev, P. Modisha and D. G. Bessarabov, *Int. J. Hydrogen Energy*, 2020, **45**, 26070–26079.
10 C. Li, Y. Liu, L. Guan, K. Li, G. Wang and Y. Lin, *Chem. Eng. J.*, 2020, **400**, 125884.
11 Z. P. Cano, D. Banham, S. Ye, A. Hintennach, J. Lu, M. Fowler and Z. Chen, *Nat. Energy*, 2018, **3**, 279–289.
12 M. Carmo, D. L. Fritz, J. Mergel and D. Stolten, *Int. J. Hydrogen Energy*, 2013, **38**, 4901–4934.
13 E. L. Fernandez, J. G. Rostra, J. P. Espinose, A. R. Gonzalezelipe, F. Yubero and A. D. L. Consuegra, *J. Power Sources*, 2019, **415**, 136–144.
14 M. Mandal, *ChemElectroChem*, 2021, **8**, 36–45.
15 C. G. M. Guio, L. A. Stern and X. Hu, *Chem. Soc. Rev.*, 2014, **43**, 6555–6569.
16 Y. Shi and B. Zhang, *Chem. Soc. Rev.*, 2016, **45**, 1529–1541.
17 J. A. Turner, *Science*, 2004, **305**, 972–974.
18 L. Fan, Z. Tu and S. H. Chan, *Energy Rep.*, 2021, **7**, 8421–8446.
19 J. D. Holladay, J. Hu, D. L. King and Y. Wang, *Catal. Today*, 2009, **139**, 244–260.
20 Y. Jiao, Y. Zheng, M. Jaroniec and S. Z. Qiao, *Chem. Soc. Rev.*, 2015, **44**, 2060–2086.
21 A. S. Batchellor and S. W. Boettcher, *ACS Catal.*, 2015, **5**, 6680–6689.
22 Y. Wu, M. Chen, Y. Han, H. Luo, X. Su, M. T. Zhang, X. Lin, J. Sun, L. Wang, L. Deng, W. Zhang and R. Cao, *Angew. Chem., Int. Ed.*, 2018, **54**, 48–70.
23 A. Kirubakaran, S. Jain and R. K. Nema, *Renewable Sustainable Energy Rev.*, 2009, **13**, 2430–2440.
24 S. Sengodan, R. Lan, J. Humphreys, D. Du, W. Xu, H. Wang and S. Tao, *Renewable Sustainable Energy Rev.*, 2018, **82**, 761–780.

25 S. Verhelst and T. Wallner, *Science*, 2009, **35**, 490–527.
26 L. Mingchuan and G. Shaojun, *Nat. Rev. Mater.*, 2017, **2**, 11059.
27 N. Shaari and S. K. Kamarudin, *Renew. Sustain. Energy Rev.*, 2017, **69**, 862–870.
28 Z. Wang, X. Meng, X. Li, J. Du, S. Li, Z. Jiang and T. Tang, *J. Phys. Chem. C*, 2009, **113**, 8058–8064.
29 Z. Q. Liu, H. Cheng, N. Li, T. Y. Ma and Y. Z. Su, *Adv. Mater.*, 2016, **28**, 3777–3784.
30 J. Kibsegaard and T. F. Jaramillo, *Angew. Chem., Int. Ed.*, 2014, **53**, 14433–14437.
31 C. Y. Su, A. Y. Lu, Y. Xu, F. R. Chen, A. N. Khlobystov and L. J. Li, *ACS Nano*, 2011, **5**, 2332–2339.
32 D. I. Zhao, Z. Zhuang, X. Cao, C. Zhang, Q. Peng, C. Chen and Y. Li, *Chem. Soc. Rev.*, 2020, **49**, 2215–2264.
33 S. Pei, Q. Wei, K. Huang, H. M. Cheng and W. Ren, *Nat. Commun.*, 2018, **9**, 145.
34 J. Miao, X. Teng, R. Zhang, P. Guo, Y. Chen, X. H. Zhou, H. Wang, X. Sun and L. Zhang, *Appl. Catal., B*, 2020, **263**, 118109.
35 L. Yi, B. Feng, N. Chen, W. Li, J. Li, C. Fang, Y. Yao and W. Hu, *Chem. Eng. J.*, 2021, **415**, 129034.
36 A. Saad, H. Shen, Z. Cheng, Q. Ju, H. Guo, M. Munir, A. Turak, J. Wang and M. Yang, *ACS Appl. Energy Mater.*, 2020, **3**, 1684–1693.
37 J. E. Park, M. J. Kim, M. S. Lim, S. Y. Kang, J. K. Kim, S. H. Oh, M. Her, Y. H. Cho and Y. E. Sung, *Appl. Catal., B*, 2018, **237**, 140–148.
38 T. Zhang, F. Song, Y. Qian, H. Gao, J. Shaw and Y. Rao, *ACS Appl. Energy Mater.*, 2021, **4**, 5434–5454.
39 L. Fan, P. F. Liu, X. Yan, L. Gu, Z. Z. Yang, H. Y. Yang, S. Qiu and X. Yao, *Nat. Commun.*, 2016, **7**, 10667.
40 M. Li, J. Wang, X. Guo, J. Li, Y. Huang, S. Geng, Y. Yu, Y. Liu and W. Yang, *Appl. Surf. Sci.*, 2021, **536**, 147909.
41 A. J. J. Amalraj and S. F. Wang, *J. Ind. Eng. Chem.*, 2022, **111**, 356–368.
42 M. Nemiwal, T. C. Zhang and D. Kumar, *Carbohydr. Polym. Technol. Appl.*, 2021, **2**, 100164.
43 Z. Wen, H. Li, H. Li, H. Huo, F. Wang, Y. Gu, Y. Yang and J. Zhao, *J. Power Sources*, 2021, **509**, 230370.
44 A. T. Erturk, U. Ergin, T. Kadioglu, A. C. Turkman and C. Celik, *Int. J. Hydrogen Energy*, 2022, **47**, 23373–23380.
45 M. Carvela, G. O. S. Santos, I. M. D. Gonzaga, K. I. B. Eguiluz, J. Lobato, G. R. S. Banda and M. A. Rodrigo, *Int. J. Hydrogen Energy*, 2021, **46**, 32602–32611.
46 Y. Arafat, M. R. Azjar, U. Zhong, M. O. Tade and Z. Shao, *Mater. Res. Bull.*, 2021, **140**, 111315.
47 L. Dai, Y. Xue, L. Qu, H. J. Choi and J. B. Baek, *Chem. Rev.*, 2015, **115**, 4823–4892.
48 M. Zulqarnain, A. Shah, M. A. Khan, F. J. Iftikhar and J. Nisar, *Sci. Rep.*, 2020, **10**, 6328.
49 P. Xu, J. Li, J. Lue, L. Wei, D. Zhang, D. Zhou, W. Xu and D. Yuan, *Sci. Rep.*, 2018, **8**, 9425.
50 N. K. Oh, J. Seo, S. Lee, H. J. Kim, U. Kim, J. Lee, Y. K. Han and H. Park, *Nat. Commun.*, 2021, **12**, 4606.
51 D. N. Nguyen, G. S. Gund, M. G. Jung, S. H. Roh, J. Park, J. K. Kim and H. S. Park, *ACS Nano*, 2020, **14**, 17615–17625.
52 A. T. Swesi, J. Masuol, W. P. R. Liyanage, S. Umapathi, E. Bohannan, J. Madvedeva and M. Nath, *Sci. Rep.*, 2017, **7**, 2401.
53 J. Hou, Y. Wu, S. Cao, Y. Sun and L. Sun, *Small*, 2017, **13**, 1702018.
54 X. Zhang, T. Liu, T. Guo, Z. Mu, X. Hu, K. He, X. Chen, V. P. David and Z. W. D. Wang, *ACS Appl. Mater. Interfaces*, 2021, **34**, 40705–40712.
55 A. K. Manohar, C. Yang and S. Narayanan, *J. Electrochem. Soc.*, 2015, **162**, A1864.
56 X. Rui, H. Tan and Q. Yan, *Nanoscale*, 2014, **6**, 9889–9924.
57 I. K. Ahn, W. Joo, J. H. Lee, H. G. Kim, S. Y. Lee, Y. Jung, J. Y. Kim, G. B. Lee, M. Kim and Y. C. Joo, *Sci. Rep.*, 2019, **9**, 19539.
58 H. Li, S. Chen, Y. Zhang, Q. Zhang, X. Jia, Q. Zhang, L. Gu, X. Sun, L. Song and X. Wang, *Nat. Commun.*, 2018, **9**, 2452.
59 S. Czioska, J. Wang, X. Teng and Z. Chen, *ACS Sustainable Chem. Eng.*, 2018, **6**, 11877–11883.
60 A. Sathyaseelan, D. Kesavan, S. Manoharan, V. K. Mariappan, K. Krishnamoorthy and S. J. Kim, *ACS Appl. Energy Mater.*, 2021, **4**, 7020–7029.
61 K. Srinivas, Y. Chen, X. Wang, B. Wang, B. Wang, M. Karpuraranjith, W. Wang, Z. Su, W. Zhang and D. Yang, *ACS Sustainable Chem. Eng.*, 2021, **9**, 1920–1931.
62 X. Wu, X. Han, X. Ma, W. Zhang, Y. Deng, C. Zhong and W. Hu, *ACS Appl. Mater. Interfaces*, 2017, **9**, 12574–12583.
63 K. Santhosh Kumar, G. L. Prajapati, R. Dagar, M. Vagadia, D. S. Rana and M. Tonouchi, *Adv. Opt. Mater.*, 2020, **8**, 1900958.
64 Y. Tokura, Correlated-Electron Physics in Transition Metal Oxides, *Phys. Today*, 2003, **56**, 50.
65 E. Morosan, D. Natelson, A. H. Nevidomskyy and Q. Si, *Adv. Mater.*, 2012, **24**, 4896–4923.
66 C. N. R. Rao, *Transition-metal oxides*, United States, Marcel Dekker, Inc, 1974.
67 T. Guo, M. S. Yao, Y. H. Lin and C. W. Nan, *CrystEngComm*, 2015, **17**, 3551–3585.
68 C. Yuan, H. B. Wu, Y. Xie and X. W. Lou, *Angew. Chem., Int. Ed.*, 2014, **53**, 1488–1504.
69 V. E. Henrich and P. A. Cox, *The Surface Science of Metal Oxides*, Cambridge University Press, Cambridge, 1994.
70 M. T. Noori, P. Chatterjee, M. M. Ghangrekar and C. K. Mukherjee, Low-Cost Solutions for Fabrication of Microbial Fuel Cells: Ceramic Separator and Electrode Modifications, *Progress and Recent Trends in Microbial Fuel Cells*, Chapter 7, 2018, 95–124.
71 D. Linden and T. B. Reddy, *Handbook of Batteries*, McGraw-Hill Professional, 2011.
72 Q. Liu, Z. F. Li, Y. Liu, H. Zhang, Y. Ren, C. J. Sun, W. Lu, Y. Zhou, L. Stanciu and E. A. Stach, *Nat. Commun.*, 2015, **6**, 6127.
73 Y. Zhang and S. J. Park, *Carbon*, 2017, **122**, 287–297.
74 G. P. Ohja, B. Pant, S. J. Park, M. Park and H. Y. Kim, *J. Colloid Interface Sci.*, 2017, **494**, 338–344.
75 H. Chen and D. Yi, *APL Mater.*, 2021, **9**, 060908.

76 Y. Ou, Z. Wang, C. S. Chang, H. P. Nair, H. Paik, N. Reynolds, D. C. Ralph, D. A. Muller, D. G. Schlom and R. A. Buhrman, *Nano Lett.*, 2019, **19**, 3663–3670.
77 A. Bose, J. N. Nelson, X. S. Zhang, P. Jadaun, R. Jain, D. G. Schlom, D. C. Ralph, D. A. Muller, K. M. Shen and R. A. Buhrman, *ACS Appl. Mater. Interfaces*, 2020, **12**, 55411–55416.
78 J. He, P. Wu, L. Lu, H. Li, H. Ji, M. He, Q. Jia, M. Q. Hua, W. Zhu and H. M. Li, *ACS Appl. Mater. Interfaces*, 2019, **11**, 36666–36675.
79 I. B. Romero, D. Sylla, M. Placidi, Y. Sanchez, J. A. Andrade Arvizu, V. Izquierdo Roca, M. Guc, A. Perez Rodriguez, S. Grini, L. Vines, B. Pusay, R. Almache, J. Puigdollers, P. Pistor, E. Saucedo and M. Espindola Rodriguez, *ACS Appl. Mater. Interfaces*, 2020, **12**, 33656–33669.
80 M. Xie, R. Luo, J. Lu, R. Chen, F. Wu, X. Wang, C. Zhan, H. Wu, H. M. Albishri, A. S. Al-Bogami, D. A. El-Hady and K. Amine, *ACS Appl. Mater. Interfaces*, 2014, **6**, 17176–17183.
81 Q. T. Phan, K. C. Poon and H. Sato, *Int. J. Hydrogen Energy*, 2021, **46**, 14190–14211.
82 W. Cheng, L. Sun, X. He and L. Tian, *Dalton Trans.*, 2022, **51**, 7763–7774.
83 V. Hasannaeimi and S. Mukherjee, *Sci. Rep.*, 2019, **9**, 1–8.
84 Z. P. Wu, D. T. Caracciolo, Y. Maswadeh, J. Wen, Z. Kong, S. Shan, J. A. Vargas, S. Yan, E. Hopkins, K. Park and A. Sharma, *Nat. Commun.*, 2021, **12**, 1–14.
85 Z. Liu, X. Yang, B. Lu, Z. Shi, D. Sun, L. Xu, Y. Tang and S. Sun, *Appl. Catal., B*, 2019, **243**, 86–93.
86 S. S. Li, J. J. Lv, L. N. Teng, A. J. Wang, J. R. Chen and J. J. Feng, *ACS Appl. Mater. Interfaces*, 2014, **6**, 10549–10555.
87 J. X. Feng, Q. L. Zhang, A. J. Wang, J. Wei, J. R. Chen and J. J. Feng, *Electrochim. Acta*, 2014, **142**, 343–350.
88 R. Arukula, M. Vinothkannan, A. R. Kim and D. J. Yoo, *J. Alloys Compd.*, 2019, **771**, 477–488.
89 D. Y. Chung, K. J. Lee and Y. E. Sung, *J. Phys. Chem.*, 2016, **120**, 9028–9035.
90 X. Fu, C. Wan, Y. Huang and X. Duan, *Adv. Funct. Mater.*, 2022, **32**, 2106401.
91 C. Wang, C. An, C. Qin, H. Gomaa, Q. Deng, S. Wu and N. Hu, *Nanomaterials*, 2022, **12**, 2480.
92 P. L. Kharel, P. M. Cullier, K. Fernando, F. P. Zamborini and B. W. Alphenaar, *J. Phys. Chem. C*, 2018, **122**, 15090–15096.
93 A. S. Patil and U. J. Tupe, *Chem. Phys. Lett.*, 2022, **796**, 139555.
94 G. A. M. Hussein, *J. Anal. Appl. Pyrolysis.*, 1996, **37**, 111–149.
95 P. Ilenchezhiyan, G. M. Kumar, S. Tamilselvan, T. W. Kang and D. Y. Kim, *Int. J. Energy Res.*, 2020, **44**, 1–9.
96 P. Li, M. Wang, X. Duan, L. Zheng, X. Cheng, Y. Zhang, Y. Kuang, Y. Li, Q. Ma, Z. Feng, W. Liu and X. Sun, *Nat. Commun.*, 2019, **10**, 1711.
97 Z. Fan, J. Jiang, L. Ai, Z. Shao and S. Liu, *ACS Appl. Mater. Interfaces*, 2019, **11**, 47894–47903.
98 X. Wu, Y. Yang, T. Zhang, B. Wang, H. Xu, X. Yan and Y. Tang, *ACS Appl. Mater. Interfaces*, 2019, **11**, 39841–39847.
99 W. Sun, W. Q. Zaman, C. Ma, J. Liao, C. Ge and J. Yang, *ACS Appl. Energy Mater.*, 2020, **3**, 4432–4440.
100 G. Rathnakar and H. K. Shivanand, *Int. j. innov. sci. technol.*, 2013, **2**, 548–552.
101 I. D. G. A. Subagia and Y. Kim, *J. Mech. Sci. Technol.*, 2013, **27**, 987–992.
102 A. A. J. M. Peijs, R. W. Venderbosch and P. J. Lemstra, *Composites*, 1990, **21**, 522–530.
103 M. Najafi, S. M. R. Khalili and R. Eslami-Farsani, *Iran. Polym. J.*, 2014, **23**, 767–773.
104 J. J. Luo and I. M. Daniel, *Compos. Sci. Technol.*, 2013, **63**, 1607–1616.
105 A. D. De Oliveira and C. A. G. Beatrice, Polymer Nanocomposites with Different Types of Nanofiller, in *Nanocomposites Recent Evolutions*, IntechOpen, London, UK, 2019, 6, 103.
106 S. Paszkiewicz, K. Pypec, I. Irska and E. Piesowicz, *Processes*, 2020, **8**, 1475.
107 E. OmanovicMiklicanin, A. Badnjevic, A. Kazlagic and M. Hajlovac, *Health Technol.*, 2020, **10**, 51.
108 M. M. Zagho, M. Al and A. Almaadeed, *Emergent Mater.*, 2020, **3**, 675–683.
109 Y. Haldorai and J. J. Shim, *Adv. Polym. Sci.*, 2014, **267**, 249–281.
110 H. S. Jena, H. Rijckaert, C. Krishnaraj, I. V. Driessche, P. V. Der Voort and A. M. Kaczmarek, *Chem. Mater.*, 2021, **33**, 8007–8017.
111 D. Hou, J. E. Bostwick, J. R. Shallenberger, E. S. Zofchak, R. H. Colby, Q. Liu and R. J. Hickey, *ACS Appl. Nano Mater.*, 2020, **3**, 962–968.
112 C. Wang, Q. Cui, X. Wang and L. Li, *ACS Appl. Mater. Interfaces*, 2016, **8**, 29101–29109.
113 S. G. Peera, C. Liu, A. K. Sahu, M. Selvaraj, M. C. Rao, T. G. Lee, R. Koutavarapu, J. Shim and L. Singh, *Adv. Mater. Interfaces*, 2021, **8**, 2100975.
114 Q. Wang, N. Han, A. Bokhari, X. Li, Y. Cao, S. Asif, Z. Shen, W. Si, F. Wang, J. J. Klemeš and X. Zhao, *Energy*, 2022, **255**, 124465.
115 A. Bhat, S. Anwer, K. S. Bhat, M. I. H. Mohideen, K. Liao and A. Qurashi, *npj 2D Mater. Appl.*, 2021, **5**, 61.
116 Y. Gogotsi and B. Anasori, *ACS Nano*, 2019, **13**, 8491–8494.
117 W. Gu, M. Wu, J. Xu and T. Zhao, *Int. J. Hydrogen Energy*, 2022, **47**, 17224–17232.
118 K. Mistry, Jalja, R. Lakshni, B. Tripathi, S. Shinde and P. Chandra, *Int. J. Hydrogen Energy*, 2022, DOI: **10.1016/j.ijhydene.2022.02.049**.
119 J. Geng, R. Wu, H. Bai, L. N. Chan, K. W. Ng, W. F. Lp and H. Pan, *Int. J. Hydrogen Energy*, 2022, **47**, 18725–18737.
120 V. Thirumal, R. Yuvakumar, P. Sentilkumar, G. Ravi, A. Arun, R. K. Guduru and D. Velauthapillai, *Int. J. Hydrogen Energy*, 2022, DOI: **10.1016/j.ijhydene.2021.12.045**.
121 X. Geng, Y. Liu, W. Xu, X. Huang, P. Wang, M. Zhan, G. Wen and W. Wang, *Ceram. Int.*, 2022, **48**, 20146–20157.
122 B. Cui, B. Hu, J. Liu, M. Wang, Y. Song, K. Tian, Z. Zhang and L. He, *ACS Appl. Mater. Interfaces*, 2018, **10**, 23858–23873.
123 I. Ashraf, S. Ahmad, S. Rizwan and M. Iqbal, *Fuel*, 2021, **299**, 120928.

124 V. Thirumal, R. Yuvakkumar, P. Senthilkumar, G. Ravi and D. Velauthapillai, *Fuel*, 2022, **317**, 123493.
125 B. K. Boggs, R. L. King and G. G. Botte, *Chem. Commun.*, 2009, **45**, 4859–4861.
126 Q. Zhang, D. Yan, Z. Nie, X. Qiu, S. Wang, J. Yuan, D. Su, G. Wang and Z. Wu, *ACS Appl. Energy Mater.*, 2018, **1**, 571–579.
127 L. Yang and L. Zhang, *J. Colloid Interface Sci.*, 2022, **607**, 546–555.
128 W. Yaseen, N. Ullah, M. Xie, B. A. Yusuf, Y. Xu, C. Tong and J. Xie, *Surf. Interfaces*, 2021, **26**, 101361.
129 Y. Pang, W. Xu, S. Zhu, Z. Cui, Y. Liang, Z. Li, S. Wu, C. Zhang and S. Luo, *J. Mater. Sci. Nanotechnol.*, 2021, **82**, 96–104.
130 X. Lu and C. Zhao, *Nat. Commun.*, 2015, **6**, 6616.
131 W. Deng, W. Xie, D. Li, Y. Gai, J. Yu, R. Yang, X. Bao and F. Jiang, *NPG Asia Mater.*, 2022, **14**, 25.
132 S. Dilpzir, P. Ren, R. Liu, M. Yuan, M. Imran, Z. Liu, Y. Xie, H. Zhao, Y. Yang, X. Wang, C. Streb and G. Zhang, *ACS Appl. Mater. Interfaces*, 2020, **12**, 23017–23027.
133 A. Muthurasu, B. Dahal, T. Mukhiya, K. Chhetri and H. Y. Kim, *ACS Appl. Mater. Interfaces*, 2020, **12**, 41704–41717.
134 G. Wei, J. He, W. Zhang, X. Zhao, S. Qiu and C. An, *Inorg. Chem.*, 2018, **57**, 7380–7389.
135 Z. Wang, B. Xiao, Z. Lin, Y. Xu, Y. Lin, F. Meng, Q. Zhang, B. Fang, L. Gu, S. Guo and W. Zhang, *Angew. Chem., Int. Ed.*, 2021, **60**, 23388–23393.
136 Y. Xue, D. Pan, F. Zuo, S. Xiao, X. Li, F. Lou, M. Li and Y. Ouyang, *RSC Adv.*, 2022, **12**, 17012–17019.
137 L. Lu and S. Z. B. Fang, *ACS Catal.*, 2021, **11**, 6020–6058.
138 B. Lu, L. Guo, F. Wu, Y. Peng, J. E. Lu, J. Smart, N. Wang, Y. Z. Finfrock, D. Morris, P. Zhang, N. Li, P. Gao and Y. P. S. Chen, *Nat. Commun.*, 2019, **10**, 631.
139 D. Zhang, H. Miao, X. Wu, Z. Wang, H. Zhao, Y. Shi, X. Chen, Z. Xiao and J. L. L. Wang, *Chin. J. Catal.*, 2022, **43**, 1148–1155.
140 X. Wu, Z. Wang, D. Zhang, Y. Qin, M. Wang, Y. Han, T. Zhan, B. Yang, S. Li, J. Lai and L. Wang, *Nat. Commun.*, 2021, **12**, 4018.
141 Y. Li, X. Tan, R. K. Hocking, X. Bo, H. Ren, B. Johnnessen, S. C. Smith and C. Zhao, *Nat. Commun.*, 2020, **11**, 2720.
142 D. Zhang, H. Zhao, B. Huang, B. Li, H. Li, Y. Han, Z. Wang, X. Wu, Y. Pan, Y. Sun and J. L. L. Wang, *ACS Cent. Sci.*, 2019, **5**, 1991–1997.
143 D. Zhang, Y. Shi, H. Zhao, W. Qi, X. Chen, T. Zhan, S. Li, B. Yang, M. Sun, J. Lai and B. H. L. Wang, *J. Mater. Chem. A*, 2021, **9**, 889–893.
144 R. Q. Yao, Y. T. Zhou, H. Shi, Q. H. Zhang, L. Gu, Z. Wen, X. Y. Lang and Q. Jiang, *ACS Energy Lett.*, 2019, **4**, 1379–1386.
145 D. Nie, D. Zhang, Z. Wang, Y. Qin, X. Zhai, B. Yang and J. L. L. Wang, *Small*, 2021, **17**, 2102879.
146 X. Zhang, J. Wang, T. Guo, T. Liu, Z. Wu, L. Cavallo and Z. C. D. Wang, *Appl. Catal., B*, 2019, **247**, 78–85.
147 D. Wang, T. Liu and J. W. Z. Wu, *Carbon*, 2018, **139**, 845–852.
148 X. Zhang, T. Guo, T. Liu, K. Lv and Z. W. D. Wang, *Electrochim. Acta*, 2019, **323**, 134798.
149 T. Liu, X. Zhang, T. Guo, Z. Wu and D. Wang, *Electrochim. Acta*, 2020, **334**, 135624.
150 T. Guo, X. Zhang, T. Liu and Z. W. D. Wang, *Appl. Surf. Sci.*, 2020, **509**, 144879.
151 X. Zhang, T. Liu, T. Guo, X. Han, Z. Mu, Q. Chen, J. Jiang, J. Yan, J. Yuan, D. Wang, Z. Wu and Z. Kou, *Chin. J. Catal.*, 2021, **42**, 1798–1807.
152 X. Ren, X. Ji, Y. Wei, D. Wu, Y. Zhang, M. Ma, Z. Liu, A. Asiri, Q. Wei and X. Sun, *Chem. Commun.*, 2018, **54**, 1425–1428.
153 B. Fang, L. Daniel, A. Bonakdarpour and D. P. Wilkinson, *Adv. Mater. Interfaces*, 2022, **9**, 2200349.
154 P. Parvasi, S. Mohammad Jokar, A. Basile and A. Iulianelli, *Membranes*, 2020, **10**, 159.
155 J. Yunzhe, Z. Bowei, W. Feifei and L. Mengmeng, *IOP Conf. Ser.: Earth Environ. Sci.*, 2020, **512**, 012136.